STATISTICS, OPTIMIZATION AND INFORMATION COMPUTING
Stat., Optim. Inf. Comput., Vol. –, 2026, pp 1–25.
Published online in International Academic Press (www.IAPress.org)

Truncated Exponentiated Weibull-G Family: Theory, Inference, and Modelling of Complete and Hybrid Censored Data

Mohamed S. Eliwa [1,2], Ibrahim Elbatal [3], Hend S. Shahen [4], Mahmoud El-Morshedy [4*]

[1]*Department of Statistics and Operations Research, College of Science, Qassim University, Saudi Arabia*
[2]*Department of Mathematics, Faculty of Science, Mansoura University, Mansoura 35516, Egypt*
[3]*Department of Mathematics and Statistics, Faculty of Science, Imam Mohammad Ibn Saud Islamic University (IMSIU), Riyadh 11432, Saudi Arabia*
[4]*Department of Mathematics, College of Science and Humanities in Al-Kharj, Prince Sattam bin Abdulaziz University, Al-Kharj 11942, Saudi Arabia*

Abstract
In this paper, the truncated exponentiated Weibull-G family is introduced, and its core analytical properties are developed: the density, hazard rate function (hrf), moments, reliability measures, entropy functionals, and selected characterizations. The exponential, Rayleigh, and Lindley baselines serve to illustrate the generator. The proposed family generates flexible models capable of accommodating both symmetric and asymmetric data across varying levels of kurtosis. Its hrf admits a wide range of shapes, including monotone and non-monotone behaviour increasing, decreasing, bathtub, unimodal, J-shaped, inverse-J-shaped, and others. Estimation is investigated under complete observation and Type-I hybrid censoring through a reproducible Monte Carlo experiment comprising $48{,}000$ independently generated datasets: four parameter configurations, four sample sizes, three observation regimes, and $1{,}000$ replications per design cell. Maximum likelihood and a fixed-prior posterior mode in log-parameter coordinates are assessed throughout, with maximum product spacing evaluated separately for complete samples. Beyond bias and root mean square error, cumulative distribution function recovery, boundary solutions, the availability and conditional coverage of observed-information confidence intervals are examined. The results distinguish useful distributional recovery from persistent identifiability difficulties for individual parameters, particularly under censoring with Bayesian analysis. To test the flexibility of the new class, a lifetime data is analyzed using the exponential-baseline model and compared with three explicitly selected reference distributions, using information criteria and refitted parametric-bootstrap Kolmogorov–Smirnov p-values. The findings illustrate flexible fitting and provide a transparent assessment of point estimation and uncertainty.

Keywords statistical model; hybrid censoring; Bayesian inference; reproducible Monte Carlo simulation; truncation; goodness-of-fit.

2020 Mathematics Subject Classification: 62N01, 62N02, 62N05, 62F10, 62F15, 62G10, 62F40.

DOI: 10.19139/soic-2310-5070-4732

1. Introduction

Lifetime models are evaluated on two fronts: how well they describe the underlying failure process, and how well they accommodate the mechanism by which observations reach the analyst. The second is easily overlooked. In reliability experiments for manufacturing, failures are recorded only within a prescribed observation window; in insurance, losses below a reporting threshold never enter the claim file; in medical follow-up, individuals are enrolled only if they have already survived to a certain age; in biological studies, organisms are sampled only if they have reached a measurable stage of development; in engineering, components are tested only if they withstand an initial

*Correspondence to: Mahmoud El-Morshedy (Email: m.elmorshedy@psau.edu.sa)

ISSN 2310-5070 (online) ISSN 2311-004X (print)
Copyright © 2026 International Academic Press

screening load. In each case, the observed sample is not a random sample from the population of interest, and the distribution it represents is not the one the model specifies. Ignoring this distinction does not merely reduce efficiency: it targets the wrong likelihood, and the resulting estimates are biased in ways that no increase in sample size will remove.

Truncation and censoring capture the two ways this can happen. Truncation removes observations outside a specified region from the sample altogether, whereas censoring retains them but records their values only partially. The distinction is not merely terminological: the two mechanisms generate different likelihoods and must not be used interchangeably. For a continuous random variable with cdf H, conditioning on $a < Y \leq b$ gives the truncated cumulative distribution function (cdf)

$$H_{(a,b]}(y) = \frac{H(y) - H(a)}{H(b) - H(a)}, \qquad a < y \leq b, \tag{1}$$

provided that $H(b) > H(a)$. The consequences of this restriction have been documented across a wide range of distributional settings. Zhang and Xie [33] examined the upper-truncated Weibull distribution and its implications for reliability. Aban et al. [1] developed estimation procedures for the truncated Pareto distribution, while Zaninetti and Ferraro [32] investigated its relevance to bounded power-law phenomena. Related contributions include the truncated Birnbaum–Saunders model of Ahmed et al. [3], the truncated Lindley distributions studied by Singh et al. [31], and the truncated power-law models considered by Burroughs and Tebbens [7]. Taken together, these studies show that an upper or lower bound is never a purely technical adjustment: it changes the shape of the likelihood, the interpretation of risk, and the comparability of estimates across studies. Truncation is equally productive as a device for constructing distribution families, even when the observed response is not itself truncated. Here an auxiliary distribution is confined to the unit interval and composed with a baseline cdf, so that truncation acts on the generator rather than on the support of the response. Najarzadegan et al. [26] used this approach to develop the truncated Weibull-G family, and Jamal et al. [23] subsequently studied a truncated general-G class with an application to the truncated Burr-G family. To describe the construction, let $G(x;\boldsymbol{\varphi})$ be an absolutely continuous baseline cdf with density $g(x;\boldsymbol{\varphi})$, and let R be an auxiliary cdf with density r. Assuming $R(0) = 0$ and $R(1) > 0$, the generated cdf and density are

$$F(x) = \frac{R(G(x;\boldsymbol{\varphi}))}{R(1)}, \qquad f(x) = \frac{r(G(x;\boldsymbol{\varphi}))\, g(x;\boldsymbol{\varphi})}{R(1)}. \tag{2}$$

This reweights the baseline density through $r(G(x;\boldsymbol{\varphi}))$ while preserving its support; the beta-generated family of Eugene et al. [17] is recovered by taking a beta distribution for the unit-interval generator. The last decade has produced a steady stream of such families, and the pace has not slowed. Bashir et al. [6] introduced a bounded exponentiated Weibull distribution with quantile regression methods for mortality and survival proportions. Elghaly et al. [9] proposed the unit power generalized Weibull distribution and examined its properties, inference, and applications in medicine, engineering, and radiation. Obakeng-Maphane et al. [28] developed the Marshall–Olkin extended odd Weibull-G family for lifetime data with varied hazard structures. Abdelall et al. [2] extended the odd inverse Weibull-G family with Bayesian and non-Bayesian estimation, and Atchad et al. [5] proposed a shifted Lomax-X family for actuarial and financial data. [4] modelled inflation risk using actuarial techniques, Hassan et al. [22] developed efficient inference for the stress–strength reliability $P(W < Z)$ under ranked set sampling, and KrishnaKumari and George [24] proposed a left-truncated distribution for failure-time data that directly addresses the bias truncation induces.

The odd Weibull-G generator has become one of the most actively developed branches of the wider Weibull-G literature, and much of that development is due to several authors. In its continuous form, the generator was extended to the bivariate setting through a Marshall–Olkin shock construction built from three independent odd Weibull-G families, with maximum likelihood and Bayesian estimation and bootstrap confidence intervals developed alongside it Eliwa and El-Morshedy [10]. The same generator was then discretized for count data, yielding a family whose failure rate accommodates decreasing, increasing, constant, J- and bathtub-shaped forms El-Morshedy et al. [11]. Parallel refinements enriched the generator itself, notably a type I half-logistic odd Weibull extension El-Morshedy et al. [12] and a discrete double-factor formulation El-Morshedy and Eliwa [13]. Subsequent work has moved into new sub-models and inferential regimes: the discrete odd Weibull-Lindley distribution Shahen et al. [14], a Weibull-G-negative binomial class under hybrid censoring El-Morshedy et al. [15], and a bivariate exponentiated inverse flexible Weibull extension El-Morshedy and Eliwa [16]. Taken together, these contributions position the odd

Weibull-G framework as a versatile platform for reliability, survival and count-data modelling, and they motivate the extension pursued in the present study.

This body of work converges on a shared conclusion: the performance of a lifetime model depends jointly on the flexibility of the generator, the mechanism by which data are collected, and the inferential procedure applied to them. Yet it also leaves a question that the accumulation of new families has not answered. A generator typically enters a model as one or two additional parameters, and a richer parameter space is not by itself a contribution. What does an additional parameter actually change probabilistically and not merely dimensionally and can that change be expressed in a form that supports estimation, model comparison, and interpretation? A family that cannot answer this question invites the objection that it fits better only because it is larger. The present paper is built around that question. We take the exponentiated Weibull distribution, introduced by Mudholkar and Srivastava [25] and studied further by Pal et al. [29], as the auxiliary generator. Its cdf,

$$R(t;\lambda,\alpha,\theta)=\left(1-e^{-\lambda t^{\alpha}}\right)^{\theta},\qquad t>0,\quad \lambda,\alpha,\theta>0, \tag{3}$$

extends the Weibull through an exponentiation parameter and admits a broader range of lifetime behaviour. Restricting this auxiliary distribution to $(0,1)$ and applying (2) yields the truncated exponentiated Weibull-G (TEW-G) family:

$$F_{\text{TEW-}G}(x;\lambda,\alpha,\theta,\boldsymbol{\varphi})=\left\{\frac{1-e^{-\lambda G(x;\boldsymbol{\varphi})^{\alpha}}}{1-e^{-\lambda}}\right\}^{\theta}. \tag{4}$$

Throughout, $\lambda,\alpha,\theta>0$, and $\boldsymbol{\varphi}$ belongs to the parameter space of the baseline distribution. The choice is deliberate rather than arbitrary: because $\theta=1$ returns the truncated Weibull-G family of Najarzadegan et al. [26], the new parameter is not an addition to an unrelated construction but a nested extension of an existing one. Writing $F_{\text{TW-}G}$ for the truncated Weibull-G cdf at fixed $\lambda,\alpha,\boldsymbol{\varphi}$, (4) becomes

$$F_{\text{TEW-}G}(x)=\left\{F_{\text{TW-}G}(x)\right\}^{\theta}, \tag{5}$$

so that θ acts on the probability scale in a way that is transparent, monotone in the usual stochastic order, and interpretable through order statistics: for a positive integer $\theta=m$, the cdf is that of the maximum of m independent variables with the corresponding truncated Weibull-G distribution, and for noninteger $\theta>0$ it extends this construction continuously. The added parameter therefore carries a concrete probabilistic meaning rather than serving as a fitting convenience. Differentiating (4) gives the probability density function (pdf)

$$\begin{aligned}f_{\text{TEW-}G}(x)=&\frac{\lambda\alpha\theta\, g(x;\boldsymbol{\varphi})G(x;\boldsymbol{\varphi})^{\alpha-1}}{(1-e^{-\lambda})^{\theta}}\\&\times e^{-\lambda G(x;\boldsymbol{\varphi})^{\alpha}}\left[1-e^{-\lambda G(x;\boldsymbol{\varphi})^{\alpha}}\right]^{\theta-1}.\end{aligned} \tag{6}$$

This expression holds almost everywhere in the interior of the baseline support, with endpoint values understood through limits when needed. The transformation in (4) is increasing from zero to one, so the density is nonnegative and integrates to one; the normalizing factor $(1-e^{-\lambda})^{\theta}$ follows directly from truncating the auxiliary exponentiated Weibull variable at one. For reliability analysis, the survival function is

$$S_{\text{TEW-}G}(x)=\frac{(1-e^{-\lambda})^{\theta}-\left[1-e^{-\lambda G(x;\boldsymbol{\varphi})^{\alpha}}\right]^{\theta}}{(1-e^{-\lambda})^{\theta}}. \tag{7}$$

Consequently, the hrf, defined wherever $S_{\text{TEW-}G}(x)>0$, is

$$\begin{aligned}h_{\text{TEW-}G}(x)=&\frac{\lambda\alpha\theta\, g(x;\boldsymbol{\varphi})G(x;\boldsymbol{\varphi})^{\alpha-1}e^{-\lambda G(x;\boldsymbol{\varphi})^{\alpha}}}{(1-e^{-\lambda})^{\theta}-\left[1-e^{-\lambda G(x;\boldsymbol{\varphi})^{\alpha}}\right]^{\theta}}\\&\times\left[1-e^{-\lambda G(x;\boldsymbol{\varphi})^{\alpha}}\right]^{\theta-1}.\end{aligned} \tag{8}$$

When the baseline represents a nonnegative lifetime, $S_{\text{TEW-}G}(x)$ gives the probability of survival beyond time x, while $h_{\text{TEW-}G}(x)$ describes the instantaneous failure rate conditional on survival to that time. The same formulas remain valid for other absolutely continuous baselines, although a lifetime interpretation then requires an appropriate support. The aim of this paper is to develop the TEW-G construction and to assess whether its additional structure offers a defensible balance between distributional adaptability and inferential tractability. The new class can be

applied across a wide range of fields, including medicine and public health, where it serves to model survival and healthy-lifetime outcomes; actuarial science, for claims severity, loss distributions and life contingencies; engineering and astronomy, for component failure times, fatigue life and the modelling of astronomical event durations and waiting times; and renewable energy and manufacturing, for the lifetime of wind turbines, photovoltaic modules and other critical assets, as well as for reliability and warranty analysis.

The remainder of the paper is organized as follows. Section 2 presents the distinctive models it generates. Section 3 develops the probability-scale representation of the TEW-G law and examines the family's statistical properties, along with its characterizations. Estimation methods are discussed in Section 4, followed by the simulation study in Section 5. Section 6 presents the data application, and Section 7 concludes the paper.

2. Special Cases of the TEW-*G* Family

This section presents three specific models belonging to the TEW-G family. The density in (6) is easier to work with whenever the baseline cdf $G(x;\boldsymbol{\varphi})$ and density $g(x;\boldsymbol{\varphi})$ have closed-form expressions, so each submodel is fully determined once the baseline pair (G, g) is fixed. We obtain three submodels by taking the exponential, Rayleigh, and Lindley distributions as baselines. Their cdfs and densities are listed in Table 1. Throughout, $\boldsymbol{\varphi}$ is the scalar parameter of the selected baseline. Two features of Table 1 are worth noting before the submodels are introduced. The Lindley baseline is a two-component mixture: it is the distribution of an exponential variable with rate a and a gamma variable with shape 2 and rate a, mixed in proportions $a/(1+a)$ and $1/(1+a)$. Its density can be increasing near the origin or decreasing throughout, depending on the value of a. The exponential and Rayleigh baselines are distinct fixed-shape members of the Weibull family, corresponding respectively to shapes one and two. This provides complementary hazard patterns for the generated submodels.

Table 1. Baseline distributions are used to define the TEW-G submodels.

Model	$G(x;\boldsymbol{\varphi})$	$g(x;\boldsymbol{\varphi})$	Parameter space
Exponential	$1-e^{-\beta x}$	$\beta e^{-\beta x}$	$\beta>0$
Rayleigh	$1-e^{-\frac{\rho}{2}x^2}$	$\rho x e^{-\frac{\rho}{2}x^2}$	$\rho>0$
Lindley	$1-\left(1+\dfrac{ax}{1+a}\right)e^{-ax}$	$\dfrac{a^2}{1+a}(1+x)e^{-ax}$	$a>0$

2.1. Truncated exponentiated Weibull exponential (TEWEx) distribution

The exponential distribution describes the time between events in a Poisson process, where events occur continuously and independently at a constant average rate. Substituting $G(x;\beta)=1-e^{-\beta x}$ into (4) and (6), the cdf of the truncated exponentiated Weibull exponential (TEWEx) model is

$$F_{\mathrm{TEWEx}}(x;\lambda,\alpha,\theta,\beta)=\frac{\left\{1-e^{-\lambda(1-e^{-\beta x})^{\alpha}}\right\}^{\theta}}{(1-e^{-\lambda})^{\theta}},\qquad x>0, \tag{9}$$

and the corresponding density is

$$\begin{aligned} f_{\mathrm{TEWEx}}(x;\lambda,\alpha,\theta,\beta)=&\frac{\lambda\alpha\theta\beta\, e^{-\beta x}(1-e^{-\beta x})^{\alpha-1}}{(1-e^{-\lambda})^{\theta}}\\ &\times e^{-\lambda(1-e^{-\beta x})^{\alpha}}\left\{1-e^{-\lambda(1-e^{-\beta x})^{\alpha}}\right\}^{\theta-1},\qquad x>0, \end{aligned} \tag{10}$$

where $\lambda,\alpha,\theta,\beta>0$. The normalising factor $(1-e^{-\lambda})^{-\theta}$ remains in the density for all $\lambda>0$. With $\alpha=\theta=1$ and $\lambda\downarrow 0$, the generated cdf converges to $G(x;\beta)$, recovering the exponential baseline as a boundary limit. The same probability-scale limiting argument recovers the corresponding baseline cdfs in the submodels below. The survival and hazard rate functions (hrfs) follow from (7) and (8) with $G(x;\beta)=1-e^{-\beta x}$ and $g(x;\beta)=\beta e^{-\beta x}$, and are not restated here. Figure 1 displays the density and hazard rate of the TEWEx model for several parameter combinations. The density accommodates asymmetric shapes and, for suitable α and θ, nearly symmetric ones. The displayed

hazard curves illustrate parameter-dependent variation in the initial failure rate, subsequent trend, and location of any interior maximum; the figure is illustrative rather than an exhaustive classification of the family.

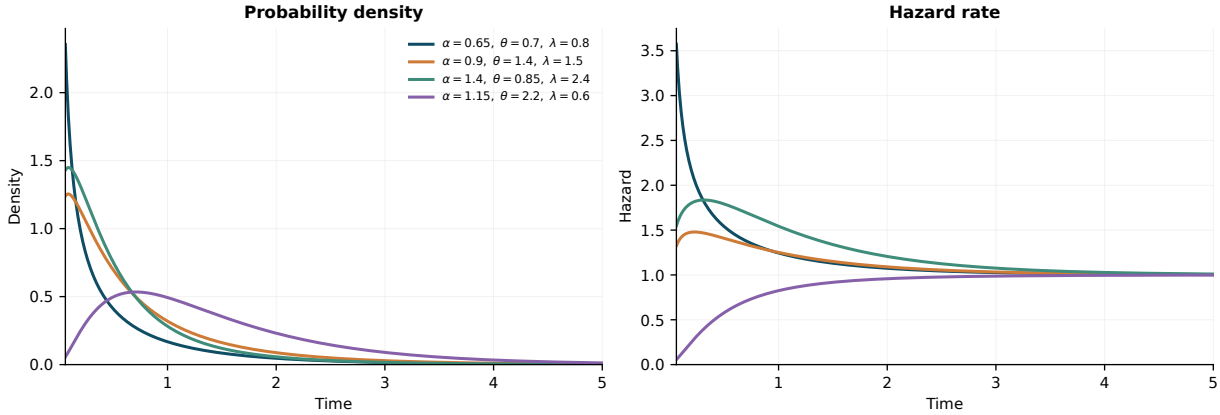


Figure 1. TEWEx density and hazard functions.

2.2. *Truncated exponentiated Weibull Rayleigh (TEWR) distribution*

The Rayleigh distribution is a continuous probability distribution that is often used to model the magnitude of random variables with positive values. Inserting the Rayleigh baseline into the generator gives

$$F_{TEWR}(x;\lambda,\alpha,\theta,\rho) = \frac{\left(1-e^{-\lambda(1-e^{-\frac{\rho}{2}x^2})^{\alpha}}\right)^{\theta}}{(1-e^{-\lambda})^{\theta}};\ x>0. \tag{11}$$

The corresponding pdf can be formulated as

$$\begin{aligned} f_{TEWR}(x;\lambda,\alpha,\theta,\rho) = {} & \frac{\lambda\alpha\theta\rho\, x\, e^{-\frac{\rho}{2}x^2}\left(1-e^{-\frac{\rho}{2}x^2}\right)^{\alpha-1}}{(1-e^{-\lambda})^{\theta}} e^{-\lambda\left(1-e^{-\frac{\rho}{2}x^2}\right)^{\alpha}} \\ & \times\left(1-e^{-\lambda\left(1-e^{-\frac{\rho}{2}x^2}\right)^{\alpha}}\right)^{\theta-1};\ x>0. \end{aligned} \tag{12}$$

Figure 2 illustrates the TEWR density and hazard curves under several parameter settings; changes in the curves reflect the combined influence of the Rayleigh baseline and the three generator parameters.

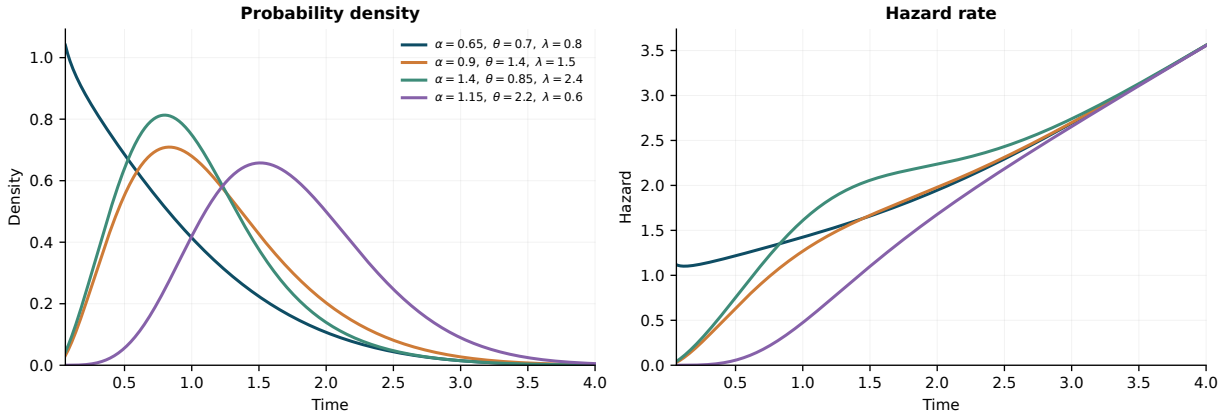


Figure 2. TEWR density and hazard functions.

2.3. Truncated exponentiated Weibull Lindley (TEWL) distribution

The Lindley distribution, commonly applied in reliability and survival analysis, serves as a probability distribution for modeling waiting times or durations. Using the Lindley baseline in the generated cdf gives

$$F_{TEWL}(x;\lambda,\alpha,\theta,a) = \frac{\left(1-e^{-\lambda\left(1-\left(1+\frac{ax}{1+a}\right)e^{-ax}\right)^{\alpha}}\right)^{\theta}}{(1-e^{-\lambda})^{\theta}};\ x>0.$$

The corresponding pdf can be reported as

$$\begin{aligned} f_{TEWL}(x;\lambda,\alpha,\theta,a) = {} & K(x;\lambda,\alpha,\theta,a)\, e^{-\lambda\left(1-\left(1+\frac{ax}{1+a}\right)e^{-ax}\right)^{\alpha}} \\ & \times \left(1-e^{-\lambda\left(1-\left(1+\frac{ax}{1+a}\right)e^{-ax}\right)^{\alpha}}\right)^{\theta-1};\ x>0, \end{aligned}$$

where

$$\begin{aligned} K(x;\lambda,\alpha,\theta,a) = {} & \frac{\lambda\alpha\theta\,\frac{a^2}{1+a}(1+x)\,e^{-ax}}{(1-e^{-\lambda})^{\theta}} \\ & \times \left(1-\left(1+\frac{ax}{1+a}\right)e^{-ax}\right)^{\alpha-1}. \end{aligned}$$

Figure 3 displays the TEWL densities and hazard functions for representative parameter combinations, illustrating the range of shapes generated from this baseline.

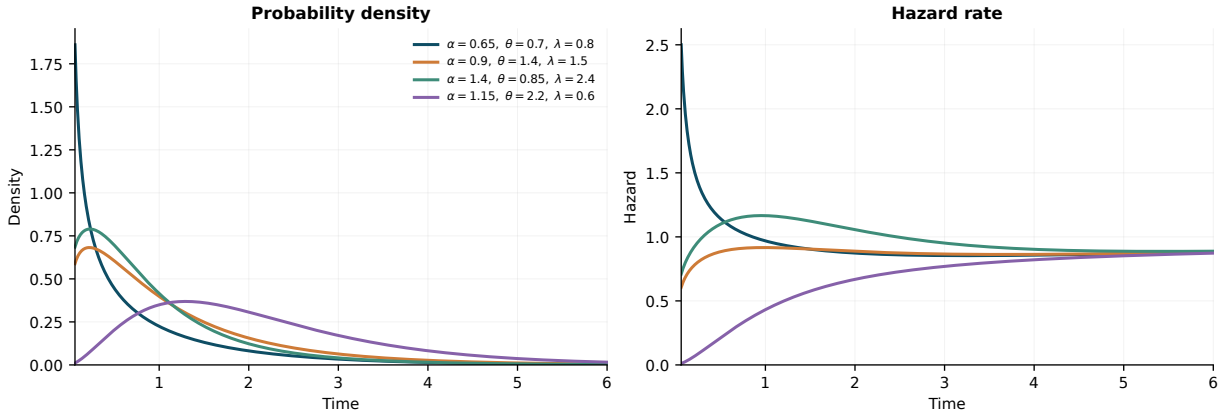


Figure 3. TEWL density and hazard functions.

3. Distributional and Reliability Properties

3.1. Probability-Scale Representation and Analytical Foundations

The generated law has a direct representation on the probability scale. For a strictly increasing baseline cdf G, set $U = G(X;\boldsymbol{\varphi})$. Then U has cdf

$$H(u) = \left\{\frac{1-\exp(-\lambda u^{\alpha})}{1-\exp(-\lambda)}\right\}^{\theta}, \qquad 0<u<1, \tag{13}$$

and density

$$w(u) = \frac{\lambda\alpha\theta}{(1-e^{-\lambda})^{\theta}} u^{\alpha-1} e^{-\lambda u^{\alpha}} (1-e^{-\lambda u^{\alpha}})^{\theta-1}, \qquad 0<u<1. \tag{14}$$

Indeed, differentiating H gives w, and $\int_0^1 w(u)\,du = H(1)-H(0) = 1$. The original density factorizes as

$$f(x;\boldsymbol{\psi}) = g(x;\boldsymbol{\varphi})\, w\{G(x;\boldsymbol{\varphi})\}. \tag{15}$$

Consequently, for any measurable ϕ with finite expectation,

$$E\{\phi(X)\} = \int_0^1 \phi\{Q_G(u)\}\, w(u)\, du. \tag{16}$$

where $Q_G(u)$ is the quantile function of the baseline G.

3.2. Moments and generating functions

For integer $r \geq 0$, when the relevant moment exists, the rth raw moment follows directly from (16):

$$\mu'_r = E(X^r) = \int_0^1 Q_G(u)^r w(u)\, du. \tag{17}$$

In particular, $\mu = \mu'_1$ and $\mathrm{Var}(X) = \mu'_2 - (\mu'_1)^2$. The central moments may be recovered by

$$\mu_r = \sum_{j=0}^{r} \binom{r}{j} (-\mu'_1)^{r-j} \mu'_j, \tag{18}$$

which gives the conventional measures of skewness and kurtosis whenever μ_4 exists. The moment generating function, on its domain of finiteness, is

$$M_X(t) = \int_0^1 \exp\{tQ_G(u)\} w(u)\, du. \tag{19}$$

These bounded-domain representations are suitable for numerical quadrature; existence of a moment depends on the tail of the baseline distribution.

3.3. Incomplete moments and residual lifetime

For a nonnegative baseline and $r > 0$, define the lower incomplete moment $\omega_r(x) = E[X^r \mathbf{1}\{X \leq x\}]$. Then

$$\omega_r(x) = \int_0^{G(x;\boldsymbol{\varphi})} Q_G(u)^r w(u)\, du. \tag{20}$$

The first incomplete moment ω_1 yields, whenever the mean is finite, the mean residual life and mean inactivity time:

$$m(x) = E(X - x \mid X > x) = \frac{\mu'_1 - \omega_1(x)}{S(x)} - x, \qquad S(x) > 0, \tag{21}$$

$$i(x) = E(x - X \mid X \leq x) = x - \frac{\omega_1(x)}{F(x)}, \qquad F(x) > 0. \tag{22}$$

Such residual-life functionals are standard in reliability theory; see Gupta and Gupta [20] as well as Navarro et al. [27]. They are evaluated using the closed-form F, S and the same one-dimensional quadrature as the raw moments.

3.4. Mean deviations and inequality curves

Let $M = Q_{\text{TEW-}G}(1/2)$ and assume $X \geq 0$ and $0 < \mu'_1 < \infty$; then $F(M) = 1/2$ by continuity of F. The mean absolute deviations about the mean and the median are, respectively,

$$E|X - \mu'_1| = 2\mu'_1 F(\mu'_1) - 2\omega_1(\mu'_1), \tag{23}$$

$$E|X - M| = \mu'_1 - 2\omega_1(M) + M\{2F(M) - 1\} = \mu'_1 - 2\omega_1(M), \tag{24}$$

so that the median term reduces to the familiar expression once $F(M) = 1/2$ is enforced. The two identities follow from splitting the integral at the centre $c \in \{\mu'_1, M\}$ and using $\int_0^c (c - x) f(x)\, dx = cF(c) - \omega_1(c)$ together with $\int_c^\infty (x - c) f(x)\, dx = \mu'_1 - \omega_1(c) - c\{1 - F(c)\}$; note that the median case carries the additional centre term $M\{2F(M) - 1\}$, which vanishes only for a symmetric law. For $0 < p < 1$, the Lorenz and Bonferroni curves

$$L(p) = \frac{\omega_1\{Q_{\text{TEW-}G}(p)\}}{\mu'_1}, \qquad B(p) = \frac{L(p)}{p}. \tag{25}$$

where $Q_{\mathrm{TEW-G}}$ is the quantile function of the new probability generator. Both are well defined: $p \mapsto Q_{\mathrm{TEW}\text{-}G}(p)$ is increasing, so $\omega_1\{Q_{\mathrm{TEW}\text{-}G}(p)\}$ is increasing in p with $\omega_1\{Q_{\mathrm{TEW}\text{-}G}(1)\} = \mu_1'$; hence, using $X \geq 0$,

$$0 \leq L(p) \leq L(1) = 1, \qquad L(p) \leq p, \qquad 0 \leq B(p) \leq \frac{p}{p} = 1, \tag{26}$$

where $L(p) \leq p$ is the Lorenz inequality and $B(p) \leq 1$ is its immediate consequence; neither bound requires symmetry, and both are attained exactly for a degenerate law. Each curve is obtained directly from the quantile function and the partial-moment integral, so no additional quadrature beyond that of (23) is needed.

3.5. Entropy

For $\rho > 0$, $\rho \neq 1$, the Rényi differential entropy is

$$H_\rho(X) = \frac{1}{1-\rho} \log \left[\int_0^1 w(u)^\rho g\{Q_G(u); \boldsymbol{\varphi}\}^{\rho-1} \, du \right], \tag{27}$$

provided that the integral is finite. This is obtained from $\int f(x)^\rho \, dx$ by setting $u = G(x)$, without a double-series interchange. Shannon differential entropy has the corresponding form

$$H(X) = -\int_0^1 w(u) \log[w(u) g\{Q_G(u); \boldsymbol{\varphi}\}] \, du, \tag{28}$$

whenever the integral of the absolute log-density is finite.

3.6. Characterizations

The truncated-moment method of Glänzel [18, 19] gives one characterization of the family. Let $t(x) = G(x; \boldsymbol{\varphi})^\alpha$ and define, on the interior of the support,

$$h(x) = e^{\lambda t(x)}[1 - e^{-\lambda t(x)}]^{1-\theta}, \qquad k(x) = t(x)h(x). \tag{29}$$

For X following the TEW-G law, direct integration of $h(x)f(x)$ and $k(x)f(x)$ gives

$$\frac{E[k(X) \mid X \geq x]}{E[h(X) \mid X \geq x]} = \frac{1 + t(x)}{2}. \tag{30}$$

Under the regularity and uniqueness conditions of the truncated-moment characterization theorem, the functions in (29) and the right side of (30) determine the TEW-G cdf. A second characterization is supplied by the reversed hazard rate $r_F(x) = \frac{f(x)}{F(x)}$. Conversely, integrating $F'(x)/F(x) = r_F(x)$ and imposing the upper-endpoint condition $F(x) \to 1$ recovers (4). Finally, write $\psi(x) = [1 - e^{-\lambda G(x;\boldsymbol{\varphi})^\alpha}]/[1 - e^{-\lambda}]$. Then

$$E[\psi(X) \mid X \leq x] = \frac{\theta}{\theta + 1} \psi(x). \tag{31}$$

This is followed by putting $F(x) = \psi(x)^\theta$ and using the probability-integral transform. Conversely, differentiation of the conditional expectation identity, together with ψ increasing from zero to one, yields $F(x) = \psi(x)^\theta$. This provides a direct conditional-moment characterization in the spirit of Hamedani [21].

4. Parameter Estimation

4.1. Maximum likelihood estimation

Let $\boldsymbol{\psi} = (\lambda, \alpha, \theta, \boldsymbol{\varphi}^\top)^\top$ denote the full parameter vector, where $\boldsymbol{\varphi}$ collects the baseline parameters, and let $x_1, \ldots, x_n$ be a random sample from the TEW-G family. Writing $G_i \equiv G(x_i; \boldsymbol{\varphi})$ and $g_i \equiv g(x_i; \boldsymbol{\varphi})$, the log-likelihood function

obtained from (6) is

$$\begin{aligned}\ell_n(\boldsymbol{\psi}) &= n\log\lambda + n\log\alpha + n\log\theta - n\theta\log(1-e^{-\lambda}) \\ &\quad + \sum_{i=1}^{n}\log g_i + (\alpha-1)\sum_{i=1}^{n}\log G_i \\ &\quad - \lambda\sum_{i=1}^{n}G_i^{\alpha} + (\theta-1)\sum_{i=1}^{n}\log\left(1-e^{-\lambda G_i^{\alpha}}\right).\end{aligned} \tag{32}$$

For numerical evaluation, all observed sample points must lie in the interior of the baseline support, so that $0 < G_i < 1$. This holds almost surely for a continuous distribution. The model itself permits all $\alpha, \theta, \lambda > 0$; a restriction $\alpha \geq 1$ is neither needed nor imposed. The normalising term is unproblematic for every $\lambda > 0$, since $1 - e^{-\lambda} \in (0, 1)$. The score vector $U_n(\boldsymbol{\psi}) = \partial\ell_n/\partial\boldsymbol{\psi}$ has components

$$U_n(\lambda) = \frac{n}{\lambda} - \frac{n\theta e^{-\lambda}}{1-e^{-\lambda}} - \sum_{i=1}^{n}G_i^{\alpha} + (\theta-1)\sum_{i=1}^{n}\frac{G_i^{\alpha}e^{-\lambda G_i^{\alpha}}}{1-e^{-\lambda G_i^{\alpha}}}, \tag{33}$$

$$\begin{aligned}U_n(\alpha) &= \frac{n}{\alpha} + \sum_{i=1}^{n}\log G_i - \lambda\sum_{i=1}^{n}G_i^{\alpha}\log G_i \\ &\quad + (\theta-1)\sum_{i=1}^{n}\frac{\lambda\, G_i^{\alpha}\log G_i\, e^{-\lambda G_i^{\alpha}}}{1-e^{-\lambda G_i^{\alpha}}},\end{aligned} \tag{34}$$

$$U_n(\theta) = \frac{n}{\theta} - n\log(1-e^{-\lambda}) + \sum_{i=1}^{n}\log\left(1-e^{-\lambda G_i^{\alpha}}\right), \tag{35}$$

and, for the k-th baseline parameter,

$$\begin{aligned}U_n(\varphi_k) &= \sum_{i=1}^{n}\frac{g_i'}{g_i} + (\alpha-1)\sum_{i=1}^{n}\frac{G_i'}{G_i} - \lambda\alpha\sum_{i=1}^{n}G_i^{\alpha-1}G_i' \\ &\quad + (\theta-1)\sum_{i=1}^{n}\frac{\lambda\alpha\, G_i^{\alpha-1}G_i' e^{-\lambda G_i^{\alpha}}}{1-e^{-\lambda G_i^{\alpha}}},\end{aligned} \tag{36}$$

where $g_i' = \partial g_i/\partial\varphi_k$ and $G_i' = \partial G_i/\partial\varphi_k$. In (34) and (36), differentiation is taken with respect to the indicated parameter. In particular,

$$\frac{\partial}{\partial\alpha}\left(-\lambda\sum_{i=1}^{n}G_i^{\alpha}\right) = -\lambda\sum_{i=1}^{n}G_i^{\alpha}\log G_i, \qquad \frac{\partial}{\partial\varphi_k}\left(-\lambda\sum_{i=1}^{n}G_i^{\alpha}\right) = -\lambda\alpha\sum_{i=1}^{n}G_i^{\alpha-1}G_i'.$$

For independent observations, the score can be written as $U_n(\boldsymbol{\psi}) = \sum_{i=1}^{n}u(x_i;\boldsymbol{\psi})$. For a fixed parameter dimension, its evaluation is linear in n. More generally, direct evaluation of the full score and Hessian typically requires $O(np)$ and $O(np^2)$ operations, respectively, provided that the necessary baseline quantities and their derivatives have bounded evaluation costs. An interior maximum likelihood estimate, when it exists and the log-likelihood is differentiable, must satisfy $U_n(\boldsymbol{\psi}) = \mathbf{0}$. However, a solution of the score equations is only a stationary point and need not be a local or global maximum. Numerical estimation therefore requires checking local curvature, comparing the attained log-likelihood values across multiple starting points, and examining possible boundary behaviour. The full parameter vector generally has no closed-form maximum likelihood estimator. If optimization is restricted to a numerical search domain, the resulting estimate is a constrained maximizer over that domain, rather than necessarily an unrestricted MLE. two considerations guide the numerical implementation. First, for fixed $(\lambda, \alpha, \boldsymbol{\varphi})$ and observations satisfying $0 < G_i < 1$, define

$$A_i = \frac{1-\exp(-\lambda G_i^{\alpha})}{1-\exp(-\lambda)}.$$

The terms involving θ in the log-likelihood are $n\log\theta + (\theta-1)\sum_{i=1}^{n}\log A_i$, up to terms independent of θ. Consequently,

$$\widehat{\theta}(\lambda,\alpha,\boldsymbol{\varphi}) = -\frac{n}{\sum_{i=1}^{n}\log A_i} > 0, \qquad \frac{\partial^2\ell}{\partial\theta^2} = -\frac{n}{\theta^2} < 0.$$

Thus, this solution is the unique conditional maximizer over $\theta > 0$ and can be substituted into the log-likelihood to reduce the dimension of the numerical optimization. Second, direct evaluation of expressions such as $\log(1-\exp(-z))$ can lose numerical accuracy when z is small. Stable implementations should use `expm1` and `log1p`, with suitable branches, and evaluate the log-likelihood directly rather than forming products of densities. Grouping the θ-dependent terms through $\log A_i$ also avoids unnecessary subtraction of large intermediate quantities. Profiling θ and optimizing the remaining positive parameters on a logarithmic scale can improve numerical conditioning, but neither procedure guarantees a global maximum or resolves weak identifiability.

4.2. Maximum product spacing

Following Cheng and Amin [8], maximum product spacing (MPS) provides an alternative estimation criterion based on increments of the fitted cdf between consecutive ordered observations. We assess its finite-sample behavior alongside maximum likelihood for complete observations, without presuming that one criterion uniformly dominates the other. With $G_0 \equiv G(x_{(0)}) = 0$ and $G_{n+1} \equiv G(x_{(n+1)}) = 1$, the spacing function for the TEW-G family is

$$\mathbb{S}(\boldsymbol{\psi}) = \prod_{i=1}^{n+1}\left[\frac{\left(1-e^{-\lambda G_i^{\alpha}}\right)^{\theta} - \left(1-e^{-\lambda G_{i-1}^{\alpha}}\right)^{\theta}}{(1-e^{-\lambda})^{\theta}}\right]^{1/(n+1)}, \tag{37}$$

whose logarithm is

$$\log\mathbb{S}(\boldsymbol{\psi}) = \frac{1}{n+1}\sum_{i=1}^{n+1}\log\left[\left(1-e^{-\lambda G_i^{\alpha}}\right)^{\theta} - \left(1-e^{-\lambda G_{i-1}^{\alpha}}\right)^{\theta}\right] - \theta\log(1-e^{-\lambda}). \tag{38}$$

The normalising factor remains part of every spacing and must be retained when evaluating the log objective. The MPS estimator maximises (38) jointly over the parameters, subject to positivity. Unlike the likelihood score in (35), the spacing objective does not admit an analogous closed-form profile in θ. The simulation uses multistart Nelder–Mead optimization of the complete-sample spacing objective followed by bounded L-BFGS-B polishing, with the polished solution retained only when it does not worsen the objective. These numerical steps were implemented in Python using `scipy.optimize` and the identical parameter limits applied to the other estimators. The simulated observations are continuous and unrounded; thus, there are no intentional ties. For data recorded on a coarse measurement grid, a grouped-data treatment would be preferable to silently changing duplicate values. To avoid cancellation when fitted cdf values are close, log spacings are evaluated using stable log-difference calculations.

4.3. Bayesian estimation and numerical implementation

A Bayesian analysis requires a prior whose support contains every admissible parameter value. In particular, imposing $\theta > 1$ is incompatible with the model's parameter space and with simulation settings having $\theta < 1$. For the real-data HMC analysis, independent weakly informative normal priors are assigned on the log-parameter scale:

$$\log\alpha,\ \log\theta,\ \log\lambda\ \sim N\left(\log(0.8), 1.4^2\right), \qquad \log\beta \sim N\left(0, 1.6^2\right), \tag{39}$$

where the four normal variables are independent. The separate simulation Log-MAP estimator uses $\boldsymbol{\mu} = (0, 0, \log 2, 0)$ and a common log-scale standard deviation 1.2, as specified in (44). Both priors are fixed before their respective analyses and are independent of the generating values and estimated parameters. The prior covers values both below and above one. For arbitrary continuous baselines, the prior on baseline parameters must be adapted to their support; the numerical implementation here concerns the exponential-baseline TEWEx model. Under a Type-I hybrid stopping rule, the experiment terminates at $C = \min\{T, X_{(r)}\}$, where r is the prespecified failure threshold. If $d = \#\{X_i \le C\}$ failures are observed, the right-censored likelihood, up to a parameter-free combinatorial factor, is

$$L_H(\boldsymbol{\psi}) = \left\{\prod_{i=1}^{d} f(x_{(i)};\boldsymbol{\psi})\right\}\left\{1-F(C;\boldsymbol{\psi})\right\}^{n-d}, \qquad C = \min\{T, X_{(r)}\}. \tag{40}$$

This expression must use the *realised* count d, not the nominal threshold r, whenever the time limit terminates the experiment first. The Bayesian posterior is obtained from L_H and the fixed priors in (39). Its log density on the transformed scale $\mathbf{t} = (\log\lambda, \log\alpha, \log\theta, \log\beta)$ is

$$\log\pi(\mathbf{t} \mid \mathcal{D}) = \ell_H(e^{\mathbf{t}}) - \frac{1}{2}\sum_{j=1}^{4}\left(\frac{t_j - \mu_j}{\sigma_j}\right)^2 + \text{constant}. \tag{41}$$

The point estimate under squared-error loss is the posterior mean; an equal-tailed 95% credible interval is given by the posterior 0.025 and 0.975 quantiles. We use two independently seeded Hamiltonian Monte Carlo chains with numerically computed preconditioning at the posterior mode. Step-size adaptation takes place only during warm-up. Convergence is examined using between-chain $\widehat{R}$ and within-chain effective-sample-size diagnostics; the real-data HMC inference must be interpreted alongside the diagnostic pass rates. The simulation assesses a distinct fixed-prior log-MAP point estimator rather than claiming HMC posterior means or credible intervals across 48,000 samples. This separation permits a clear comparison of likelihood-based and fixed-prior estimation procedures. The MPS benchmark is evaluated for complete observations using the usual $n+1$ fitted-cdf spacings. Under hybrid censoring, the study uses the corresponding right-censored likelihood in (40) for MLE and Log-MAP. This distinction is maintained in the simulation design and numerical tables.

5. Monte Carlo study: Accuracy, censoring and identifiability

The Monte Carlo experiment uses four sample sizes, $n \in \{50, 100, 200, 400\}$, four prespecified parameter configurations (Table 2), and three observation schemes: complete (Full), moderate hybrid censoring (H65), and lighter hybrid censoring (H90). Every configuration contains exactly $B = 1000$ independently generated samples, for a total of $4 \times 4 \times 3 \times 1000 = 48{,}000$ datasets. Results are summarized from the replication-level records generated under the prespecified design. Generating parameters deliberately include both $\theta < 1$ and $\theta > 1$ to probe different regions of the shape space. For each replication, draw independently $U_i \sim \mathrm{Uniform}(0,1)$ and set

$$X_i = -\frac{1}{\beta}\log\left[1 - \left\{-\frac{1}{\lambda}\log\bigl(1-(1-e^{-\lambda})U_i^{1/\theta}\bigr)\right\}^{1/\alpha}\right]. \tag{42}$$

The sampler was verified by substituting $Q(u)$ into F on a grid of 100 uniform probabilities, and the analytical log-likelihood gradient was checked against numerical differentiation for all three observation schemes. For Type-I hybrid censoring, the experiment is stopped at $C = \min\{T, X_{(r)}\}$ with $r = \lceil 0.90n \rceil$. Under H65, the fixed administrative limit is $T = Q_{\boldsymbol{\eta}_0}(0.65)$; under H90 it is $T = Q_{\boldsymbol{\eta}_0}(0.95)$. The fixed time limit is specified before sampling within each generating case. Its computation uses the generating parameter only to design the experiment; no true parameter enters the likelihood, starting values, priors or numerical estimators. If d failures are observed before C, the relevant likelihood, up to a parameter-free combinatorial factor, is

$$L(\boldsymbol{\eta}) \propto \prod_{i=1}^{d} f\bigl(X_{(i)};\boldsymbol{\eta}\bigr)\ [1 - F(C;\boldsymbol{\eta})]^{n-d}. \tag{43}$$

The observed event fractions and the proportions stopped by the time boundary are stored for every generated sample; censoring levels are never inferred from nominal labels alone.

Table 2. TEWEx simulation parameter settings and stopping times.

Case	α	θ	λ	β	T_{65}	T_{95}
A	0.80	0.90	1.50	1.00	0.440	1.933
B	1.50	0.65	2.50	1.30	0.397	1.357
C	0.70	2.00	3.00	0.80	0.548	2.128
D	1.30	1.60	4.00	1.10	0.531	1.479

Three point estimators are examined. The first is the ordinary maximum likelihood estimator (MLE), computed from (43) with multiple deterministic, sample-based starting points. The second is the posterior mode in *log-parameter coordinates* (Log-MAP), obtained by adding the same fixed independent Gaussian penalties to the log

likelihood in every replication:

$$\widehat{\mathbf{t}}_{\mathrm{Log-MAP}} = \arg\max_{\mathbf{t}\in\mathbb{R}^4} \left\{ \ell(e^{\mathbf{t}}) - \frac{1}{2}\sum_{j=1}^{4}\big[(t_j-\mu_j)/1.2\big]^2 \right\}, \qquad (\mu_1,\ldots,\mu_4) = (0,0,\log 2,0). \tag{44}$$

This estimator is the mode of the posterior density *in log coordinates*; it must not be confused with a posterior mean or with a posterior mode after changing the density to the original parameter coordinates. A proper fixed prior is used, independent of the generating truth and simulation fits. The third procedure is conventional MPS, retained only for complete samples to avoid treating an unvalidated censored spacing objective as a standard MPS estimator. MPS is fitted by multistart simplex search followed by local polishing, using the complete-sample spacings. All methods use positive parameters with common numerical limits $[0.025, 35]$ on each of the four coordinates; these are optimization safeguards, not claims about the statistical parameter space. We flag an estimate as at the boundary whenever a log parameter is within 0.012 of a search limit. Boundary solutions and optimiser failures are not removed from point-error summaries when estimates are finite. Solver success, boundary rates and the number of finite estimates are recorded separately to prevent success-only comparisons. Replication-level data and executable code accompany the manuscript. For a scalar parameter ζ, the reported bias and RMSE are

$$\widehat{\mathrm{Bias}}(\zeta) = \frac{1}{B}\sum_{b=1}^{B}(\widehat{\zeta}_b - \zeta_0), \tag{45}$$

$$\widehat{\mathrm{RMSE}}(\zeta) = \left[\frac{1}{B}\sum_{b=1}^{B}(\widehat{\zeta}_b - \zeta_0)^2\right]^{1/2}. \tag{46}$$

The mean bias, median absolute error and relative RMSE are also preserved in the machine-readable results. Separate predictive performance is measured on the fixed grid $u_j = 0.05, 0.10, \ldots, 0.95$ using

$$\text{cdf-RMSE} = \left[\frac{1}{19B}\sum_{b=1}^{B}\sum_{j=1}^{19}\big\{F(Q_{\boldsymbol{\eta}_0}(u_j);\widehat{\boldsymbol{\eta}}_b) - u_j\big\}^2\right]^{1/2}. \tag{47}$$

Unlike parameter RMSE, this functional reflects recovery of the fitted distribution even if different shape-parameter combinations are difficult to distinguish. With $B = 1000$, a hypothetical 95% coverage rate has a Monte Carlo standard error $\sqrt{0.95(0.05)/1000} \approx 0.0069$ before any qualification for unavailable intervals. Tables 3, 4, 5 and 6 give the unstandardized parameter RMSE for the four generating cases. Values should be compared within the same parameter column, not across parameters measured on different scales. Figure 4 presents the mean relative RMSE across the four generating cases, using a logarithmic vertical scale to show both stable and poorly identified directions without hiding extreme estimates. MPS full-sample results and numerical diagnostics are reported separately in Table 7. No method is guaranteed to dominate in every case.

Table 3. Parameter RMSE: Case A.

		α		θ		λ		β	
n	Regime	MLE	Log-MAP	MLE	Log-MAP	MLE	Log-MAP	MLE	Log-MAP
50	Full	4.25	0.30	22.84	0.41	5.56	0.91	0.44	0.31
50	H65	2.42	0.27	22.39	0.36	14.91	0.76	0.81	0.55
50	H90	5.38	0.35	23.70	0.45	10.86	0.90	0.56	0.34
100	Full	2.71	0.31	20.15	0.45	2.68	0.86	0.34	0.25
100	H65	3.47	0.31	21.19	0.48	14.06	0.74	0.87	0.72
100	H90	5.41	0.36	21.30	0.46	6.23	0.86	0.49	0.35
200	Full	1.20	0.33	17.46	0.47	1.79	0.81	0.32	0.26
200	H65	3.78	0.33	19.37	0.48	11.21	0.70	1.14	1.04
200	H90	3.65	0.33	19.39	0.45	2.79	0.81	0.54	0.44
400	Full	0.52	0.28	12.62	0.48	1.56	0.73	0.31	0.27
400	H65	4.19	0.32	18.40	0.49	7.95	0.67	1.43	1.37
400	H90	2.04	0.30	16.30	0.43	1.75	0.75	0.70	0.65

Table 4. Parameter RMSE: Case B.

		α		θ		λ		β	
n	Regime	MLE	Log-MAP	MLE	Log-MAP	MLE	Log-MAP	MLE	Log-MAP
50	Full	6.73	0.51	21.42	0.65	5.18	1.24	0.76	0.51
50	H65	3.38	0.51	21.88	0.60	16.35	0.64	0.86	0.26
50	H90	8.62	0.51	22.60	0.65	11.23	1.09	0.88	0.37
100	Full	4.27	0.51	18.31	0.64	2.80	1.19	0.64	0.46
100	H65	4.71	0.51	20.77	0.63	14.32	0.68	0.74	0.20
100	H90	8.02	0.51	19.49	0.61	7.99	1.18	0.75	0.37
200	Full	2.69	0.49	13.67	0.62	1.80	1.16	0.54	0.41
200	H65	5.46	0.49	18.15	0.60	13.66	0.76	0.70	0.18
200	H90	7.49	0.48	17.17	0.56	4.49	1.11	0.68	0.38
400	Full	0.96	0.42	8.52	0.44	1.71	1.09	0.45	0.35
400	H65	7.40	0.46	16.51	0.51	12.31	0.89	0.71	0.27
400	H90	5.15	0.44	14.21	0.48	2.04	1.08	0.65	0.41

Table 5. Parameter RMSE: Case C.

		α		θ		λ		β	
n	Regime	MLE	Log-MAP	MLE	Log-MAP	MLE	Log-MAP	MLE	Log-MAP
50	Full	2.33	0.36	23.18	0.77	2.13	1.08	0.51	0.40
50	H65	4.30	0.45	25.29	0.78	10.92	0.76	0.75	0.37
50	H90	4.93	0.42	25.49	0.77	5.56	0.99	0.66	0.40
100	Full	1.16	0.32	19.02	0.77	1.95	0.99	0.40	0.31
100	H65	4.38	0.42	23.54	0.78	8.12	0.71	0.63	0.30
100	H90	4.27	0.37	21.62	0.82	3.80	0.94	0.53	0.34
200	Full	0.38	0.24	15.59	0.82	2.17	0.86	0.31	0.24
200	H65	3.97	0.41	21.41	0.81	6.00	0.68	0.64	0.29
200	H90	1.60	0.26	18.28	0.83	2.13	0.85	0.45	0.29
400	Full	0.28	0.19	10.09	0.82	1.88	0.73	0.26	0.19
400	H65	2.98	0.33	19.61	0.87	3.16	0.67	0.60	0.27
400	H90	1.14	0.20	13.98	0.82	2.12	0.75	0.41	0.25

Table 6. Parameter RMSE: Case D.

		α		θ		λ		β	
n	Regime	MLE	Log-MAP	MLE	Log-MAP	MLE	Log-MAP	MLE	Log-MAP
50	Full	3.84	0.43	22.65	0.68	3.76	1.66	0.97	0.74
50	H65	5.66	0.43	23.32	0.50	11.67	1.17	1.08	0.47
50	H90	7.90	0.49	24.01	0.63	7.10	1.52	1.14	0.63
100	Full	2.29	0.39	16.96	0.75	2.59	1.52	0.82	0.66
100	H65	7.24	0.47	22.09	0.65	10.26	1.18	1.03	0.43
100	H90	6.59	0.43	21.02	0.71	3.93	1.54	1.04	0.66
200	Full	1.51	0.38	12.14	0.79	2.12	1.37	0.65	0.54
200	H65	7.35	0.45	19.05	0.72	7.21	1.13	1.05	0.41
200	H90	4.40	0.38	18.35	0.80	2.70	1.56	0.94	0.67
400	Full	0.48	0.33	6.06	0.72	2.30	1.18	0.51	0.41
400	H65	8.23	0.43	18.02	0.72	4.99	1.17	1.13	0.45
400	H90	1.47	0.34	14.39	0.71	2.12	1.52	0.85	0.64

Table 7. Complete-sample MPS accuracy and diagnostics.

Case	n	α RMSE	θ RMSE	λ RMSE	β RMSE	Solved (%)	Bound (%)
A	50	3.047	15.298	6.092	0.489	96.4	26.3
A	100	2.046	12.722	3.062	0.450	97.6	15.9
A	200	1.465	10.719	3.531	0.421	97.1	11.3
A	400	0.446	7.259	4.061	0.401	98.8	4.8
B	50	4.246	14.292	4.932	0.689	96.2	21.3
B	100	2.931	11.737	3.058	0.598	97.8	13.0
B	200	1.290	9.281	2.418	0.559	97.6	7.2
B	400	0.794	4.866	2.335	0.521	99.1	2.3
C	50	2.173	16.982	2.750	0.463	95.7	25.8
C	100	0.511	11.885	2.638	0.415	97.8	12.8
C	200	0.318	9.126	3.073	0.373	99.3	8.0
C	400	0.225	5.980	2.682	0.330	99.6	3.1
D	50	2.287	18.206	3.236	0.796	95.7	29.0
D	100	0.810	11.754	2.556	0.705	97.5	11.7
D	200	1.151	7.578	2.240	0.574	98.6	4.6
D	400	0.415	3.597	2.219	0.467	99.8	0.9

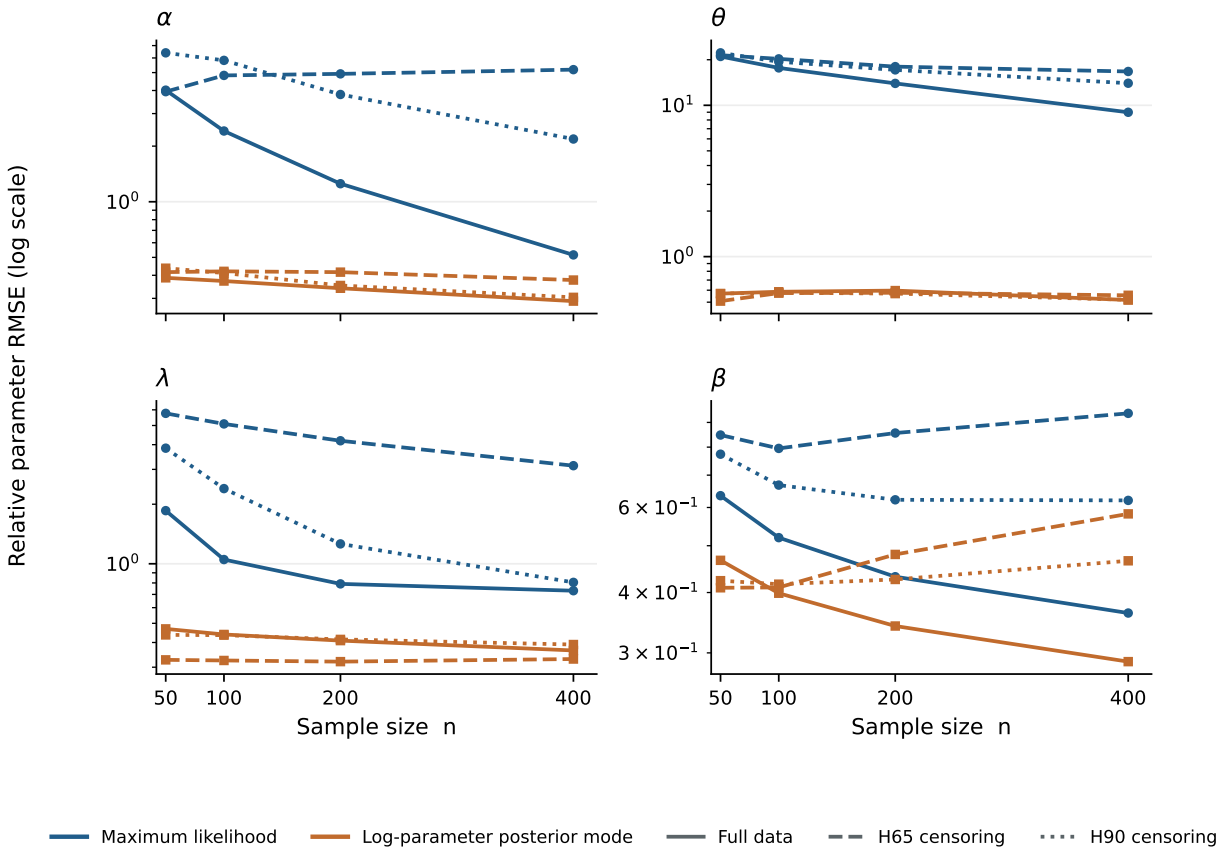


Figure 4. Relative parameter RMSE across sample sizes.

Tables 8–9 compare the cdf-grid error with the actually observed event percentage and MLE boundary rates. Figure 5 visualises distributional recovery; Figure 6 shows numerical-bound frequencies without excluding difficult replications from the error analysis. Figure 5 presents the change in cdf-RMSE across sample sizes and censoring schemes for the four generating cases. Figure 6 complements the cdf recovery results with the observed frequencies of numerical-bound estimates.

Table 8. cdf recovery and numerical diagnostics: Cases A and B.

Case	n	Regime	Events (%)	MLE cdf	Log-MAP cdf	MPS cdf	MLE bound (%)
A	50	Full	100.0	0.0514	0.0496	0.0498	51.4
A	50	H65	65.4	0.0679	0.0608	–	62.7
A	50	H90	89.9	0.0542	0.0516	–	59.5
A	100	Full	100.0	0.0368	0.0356	0.0360	36.5
A	100	H65	65.0	0.0596	0.0549	–	55.7
A	100	H90	90.0	0.0428	0.0415	–	44.2
A	200	Full	100.0	0.0292	0.0285	0.0251	26.2
A	200	H65	65.2	0.0690	0.0671	–	41.7
A	200	H90	90.0	0.0418	0.0412	–	33.7
A	400	Full	100.0	0.0264	0.0261	0.0181	12.7
A	400	H65	65.0	0.0845	0.0838	–	33.3
A	400	H90	90.0	0.0561	0.0559	–	22.0
B	50	Full	100.0	0.0502	0.0484	0.0495	44.7
B	50	H65	64.8	0.0612	0.0545	–	63.9
B	50	H90	89.9	0.0536	0.0507	–	57.3
B	100	Full	100.0	0.0364	0.0354	0.0354	30.1
B	100	H65	65.0	0.0445	0.0396	–	54.0
B	100	H90	90.0	0.0379	0.0364	–	41.5
B	200	Full	100.0	0.0254	0.0248	0.0252	15.7
B	200	H65	65.1	0.0319	0.0275	–	44.9
B	200	H90	90.0	0.0254	0.0245	–	29.8
B	400	Full	100.0	0.0199	0.0196	0.0185	5.9
B	400	H65	65.0	0.0288	0.0256	–	37.3
B	400	H90	90.0	0.0236	0.0233	–	18.2

Table 9. cdf recovery and numerical diagnostics: Cases C and D.

Case	n	Regime	Events (%)	MLE cdf	Log-MAP cdf	MPS cdf	MLE bound (%)
C	50	Full	100.0	0.0506	0.0493	0.0494	48.7
C	50	H65	65.1	0.0606	0.0538	–	68.7
C	50	H90	89.9	0.0532	0.0514	–	62.2
C	100	Full	100.0	0.0364	0.0355	0.0359	32.6
C	100	H65	64.9	0.0417	0.0369	–	54.6
C	100	H90	90.0	0.0368	0.0358	–	44.3
C	200	Full	100.0	0.0257	0.0252	0.0254	20.6
C	200	H65	65.2	0.0309	0.0273	–	42.2
C	200	H90	90.0	0.0269	0.0264	–	29.7
C	400	Full	100.0	0.0182	0.0179	0.0181	7.7
C	400	H65	65.0	0.0228	0.0202	–	34.4
C	400	H90	90.0	0.0184	0.0181	–	17.3
D	50	Full	100.0	0.0512	0.0494	0.0500	46.4
D	50	H65	65.5	0.0579	0.0523	–	61.0
D	50	H90	89.9	0.0538	0.0514	–	58.6
D	100	Full	100.0	0.0349	0.0339	0.0343	25.1
D	100	H65	64.9	0.0433	0.0381	–	53.8
D	100	H90	90.0	0.0363	0.0350	–	42.3
D	200	Full	100.0	0.0257	0.0250	0.0255	12.4
D	200	H65	64.9	0.0311	0.0271	–	38.8
D	200	H90	90.0	0.0262	0.0253	–	30.5
D	400	Full	100.0	0.0178	0.0175	0.0177	2.7
D	400	H65	65.1	0.0230	0.0197	–	33.7
D	400	H90	90.0	0.0185	0.0180	–	17.2

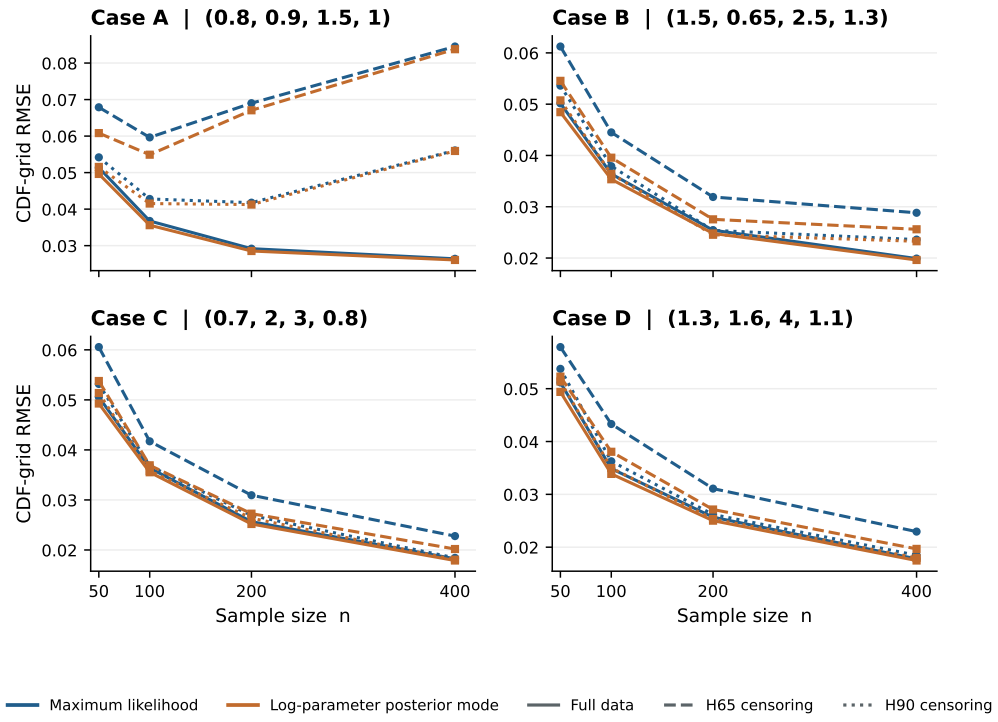


Figure 5. cdf recovery under complete and hybrid censoring.

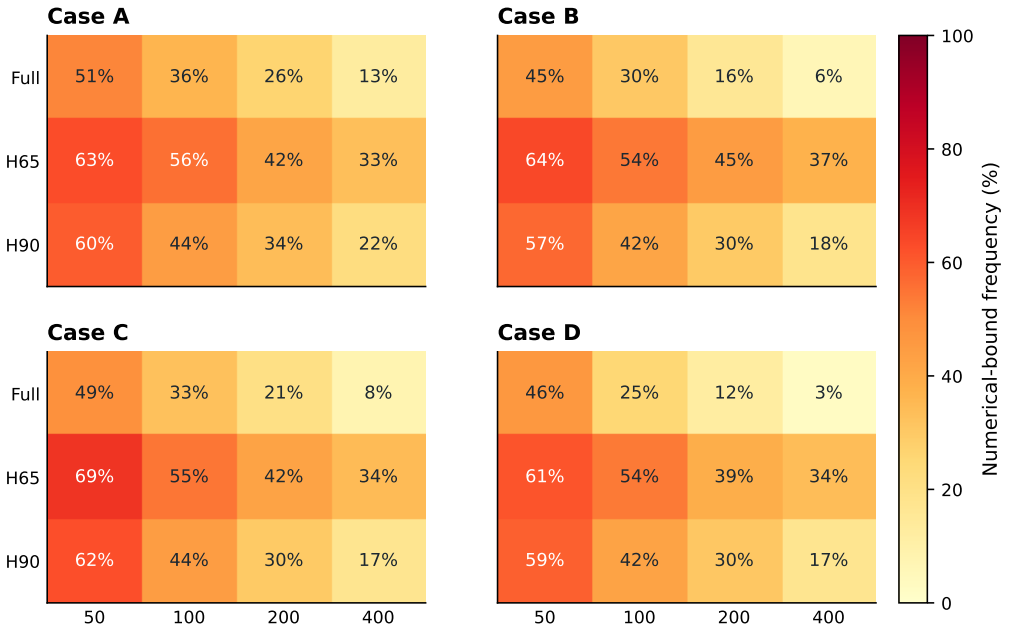


Figure 6. Frequency of numerical-bound solutions for MLE.

To assess interval estimation separately from point estimation, we conduct a frequentist coverage study based on observed information for MLE. Log-MAP is evaluated as a point estimator; no posterior-mean interval is attributed to that estimator. For each replication satisfying the solver-success and interior-solution requirements, the observed information on log-parameter coordinates is calculated by central differences of the analytical likelihood score. A nominal 95% log-Wald interval is constructed only when the information is positive definite, its smallest eigenvalue is above 10^{-6}, and its condition number is below 10^{9}.

The *validity fraction* is the percentage of all 1,000 replications where such an interval can be computed. Empirical parameter-wise coverage is reported *conditional on validity*; missing or numerically singular intervals are not counted as successful coverage. A high conditional coverage rate together with a low validity fraction does not establish reliable frequentist inference. Results appear in Tables 10– 11, with Figure 7 showing how the availability of defensible Wald intervals changes with sample size and censoring.

Table 10. Wald interval availability and coverage: Cases A and B.

Case	n	Regime	Valid (%)	α cover	θ cover	λ cover	β cover
A	50	Full	47.4	100.0	99.8	97.0	99.2
A	50	H65	36.0	100.0	100.0	100.0	100.0
A	50	H90	38.4	99.7	100.0	99.7	98.4
A	100	Full	62.9	99.7	99.4	95.9	98.6
A	100	H65	42.2	99.5	100.0	99.8	100.0
A	100	H90	53.6	99.6	100.0	100.0	99.4
A	200	Full	72.0	99.2	97.9	96.2	97.6
A	200	H65	53.2	98.5	99.8	100.0	98.7
A	200	H90	62.3	99.7	99.8	99.5	97.9
A	400	Full	82.9	97.8	97.2	94.8	96.9
A	400	H65	58.8	97.3	98.6	100.0	98.5
A	400	H90	69.7	100.0	99.7	99.7	97.3
B	50	Full	54.9	98.7	100.0	99.3	98.0
B	50	H65	36.0	100.0	100.0	100.0	100.0
B	50	H90	41.2	97.3	100.0	100.0	98.8
B	100	Full	69.7	98.6	99.6	99.0	96.1
B	100	H65	45.4	94.5	100.0	100.0	100.0
B	100	H90	58.0	97.9	100.0	100.0	97.9
B	200	Full	84.0	97.9	98.9	99.0	92.1
B	200	H65	54.8	95.1	99.1	100.0	99.3
B	200	H90	69.9	98.0	99.1	100.0	93.4
B	400	Full	93.9	97.4	98.8	97.9	92.8
B	400	H65	61.9	94.3	97.6	100.0	97.9
B	400	H90	81.2	97.5	98.0	100.0	87.8

Across the 48 design cells, the mean cdf-grid RMSE is 0.0396 for MLE and 0.0374 for the regularised Log-MAP. Log-MAP yields the smaller cdf-grid RMSE in 48 of 48 design cells; this is an *experiment-specific* result under the fixed prior, not a theorem about the superiority of a Bayesian estimator. The average MLE boundary frequency is 37.7%; averaged over cases and censoring schemes it falls from 57.1% at $n = 50$ to 20.2% at $n = 400$. Thus larger samples improve parameter separation, but the persistence of boundary solutions shows that the extra shape flexibility entails real finite-sample identifiability costs. Only 61.3% of all MLE replications, on average across cells, yield numerically admissible log-Wald intervals: the average availability increases from 42.3% at $n = 50$ to 77.9% at $n = 400$. Coverage percentages in the interval tables are *conditional* on that subset. High conditional coverage is interpreted jointly with interval length and the reported availability fraction. The coverage results correspond exclusively to the observed-information MLE intervals under the stated diagnostic conditions. These results support a nuanced practical conclusion. The fitted TEWEx cdf can be estimated reasonably in some regimes even if individual shape parameters cannot be reliably disentangled. Reporting only a small cdf error would obscure parameter uncertainty; reporting only large shape-parameter RMSE would obscure the quality of fitted probabilities. Both quantities, plus boundary incidence, censoring fractions and interval availability, are needed to assess performance. The numerical findings are conditional on the four parameter settings, predeclared stopping rules, optimisation region and fixed prior; they must not be interpreted as a uniform result for every TEW-G baseline.

Table 11. Wald interval availability and coverage: Cases C and D.

Case	n	Regime	Valid (%)	α cover	θ cover	λ cover	β cover
C	50	Full	51.3	100.0	99.4	99.4	97.1
C	50	H65	31.1	100.0	100.0	100.0	99.4
C	50	H90	37.5	100.0	99.7	100.0	98.4
C	100	Full	67.4	99.9	99.0	98.7	96.0
C	100	H65	45.1	100.0	100.0	100.0	99.8
C	100	H90	55.2	99.5	100.0	100.0	96.4
C	200	Full	79.2	99.6	98.2	97.5	95.3
C	200	H65	57.6	98.3	100.0	100.0	97.0
C	200	H90	69.9	99.4	99.9	100.0	95.3
C	400	Full	92.3	98.4	97.0	99.1	92.8
C	400	H65	65.6	99.2	99.7	100.0	93.8
C	400	H90	82.6	99.3	99.4	100.0	93.6
D	50	Full	53.5	99.6	100.0	99.8	95.0
D	50	H65	38.8	100.0	100.0	100.0	99.2
D	50	H90	41.3	100.0	100.0	100.0	97.1
D	100	Full	74.9	99.6	99.5	99.3	89.7
D	100	H65	45.5	100.0	100.0	100.0	99.1
D	100	H90	57.5	99.5	100.0	100.0	92.7
D	200	Full	87.5	99.0	99.7	99.5	87.7
D	200	H65	61.0	99.2	100.0	100.0	94.1
D	200	H90	69.4	99.0	99.6	100.0	86.9
D	400	Full	97.3	96.7	97.6	96.9	86.6
D	400	H65	66.1	98.5	99.8	100.0	91.2
D	400	H90	82.8	99.8	99.9	100.0	81.0

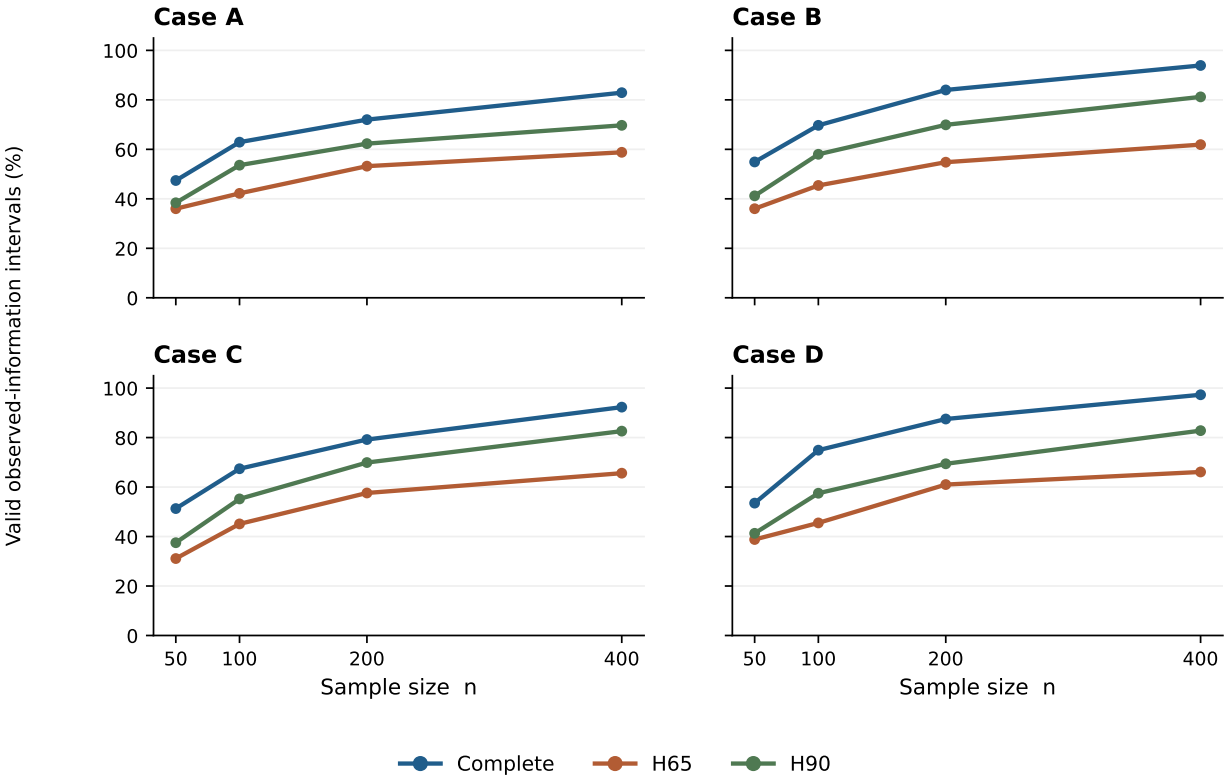


Figure 7. Availability of MLE Wald intervals.

6. Data Modelling

We re-analyze the lifetime data (minutes) reported by Shanker et al. [30]. The data, including ties introduced by measurement precision, are retained in a downloadable plain-text CSV in the reproducibility archive. For a continuous model, ties make the ordinary unmodified product-spacing objective undefined, since coincident order statistics produce zero spacings. The real-data comparison below therefore uses likelihood-based fits and a separately validated Bayesian posterior; MPS is accordingly not included in the rounded-data comparison. Figure 8 shows a right-skewed data, with an extended upper tail and departures from an exponential reference in the upper quantiles. The empirical survival and TTT panels complement this descriptive assessment.

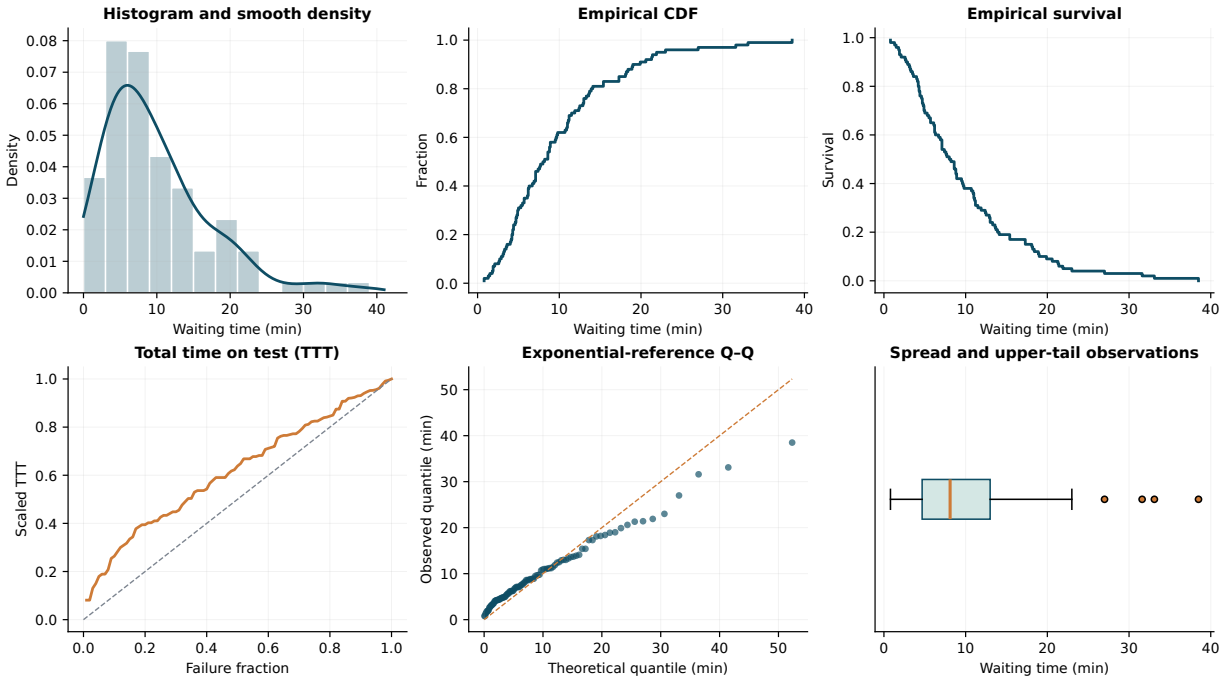


Figure 8. Exploratory summaries of data.

The positive lifetime is analyzed under the same four-model illustrative comparison, with zero location fixed for the conventional positive-support competitors. The likelihood-based criteria use the number k of estimated parameters:

$$\mathrm{AIC} = -2\widehat{\ell} + 2k, \qquad \mathrm{AICc} = \mathrm{AIC} + \frac{2k(k+1)}{n-k-1}, \qquad \mathrm{BIC} = -2\widehat{\ell} + k\log n. \tag{48}$$

In addition to these criteria we report Kolmogorov–Smirnov (KS), Anderson–Darling (AD), and Cramér–von Mises (CvM) discrepancy measures. Because the parameters are fitted using the same observations, the usual distribution-free one-sample KS p-value is not appropriate. We therefore use a model-by-model parametric bootstrap with re-fitting. For each model, $B = 1{,}999$ samples of size 100 were generated under its fitted parameters, recorded to the observed precision of 0.1 minute, and fitted again using the same estimation algorithm and bounds. The reported Monte Carlo p-value is

$$\widehat{p}_{\mathrm{KS}} = \frac{1 + \sum_{b=1}^{B} \mathbf{1}\{D_b^* \geq D_{\mathrm{obs}}\}}{B+1}, \tag{49}$$

where every D_b^* is computed after re-estimating the parameters from bootstrap sample b. This procedure accommodates estimation uncertainty and the recorded rounding, rather than treating fitted parameters as known. There were no failed bootstrap refits in the reported 1,999 draws for any model. The TEWEx model attains the smallest KS discrepancy and the largest bootstrap KS p-value in this explicitly limited comparison. Its AIC is also lower than those of the three displayed reference models; this is not a claim of superiority over every continuous

Table 12. Lifetime data model fits and bootstrap KS tests.

Model	$-\widehat{\ell}$	AIC	AICc	BIC	KS	p_{KS}	AD	CvM
TEWEx	316.960	641.921	642.342	652.341	0.038	0.9600	0.130	0.017
Lognormal	319.159	642.319	642.443	647.529	0.057	0.6260	0.408	0.054
Log-logistic	319.393	642.786	642.910	647.996	0.051	0.6570	0.315	0.035
Exponential	329.011	660.022	660.062	662.627	0.173	0.0005	4.231	0.716

lifetime distribution. The KS probabilities test each fitted distribution against the empirical sample and are not probabilities that one model is superior to another. In particular, the large p-values for several models indicate that the data do not distinguish their distribution functions sharply by this test alone. Table 12 therefore reports model rankings only within the three prespecified reference distributions. The bounded TEWEx likelihood estimate is $(\widehat{\alpha}, \widehat{\theta}, \widehat{\lambda}, \widehat{\beta}) = (0.0927, 100.0000, 2.6111, 0.1511)$. The estimate of θ reaches the imposed numerical limit. Therefore, both the information criteria and the bootstrap calibration for TEWEx pertain to the reported bounded fitting procedure; they should not be interpreted as a globally unrestricted optimum. Accordingly, the information-criterion and bootstrap results describe the fitted model under the declared optimization domain, whereas inference on individual shape parameters is interpreted with the corresponding likelihood geometry. Figure 9 compares fitted curves and probability-scale diagnostics for the same four models as in Table 12.

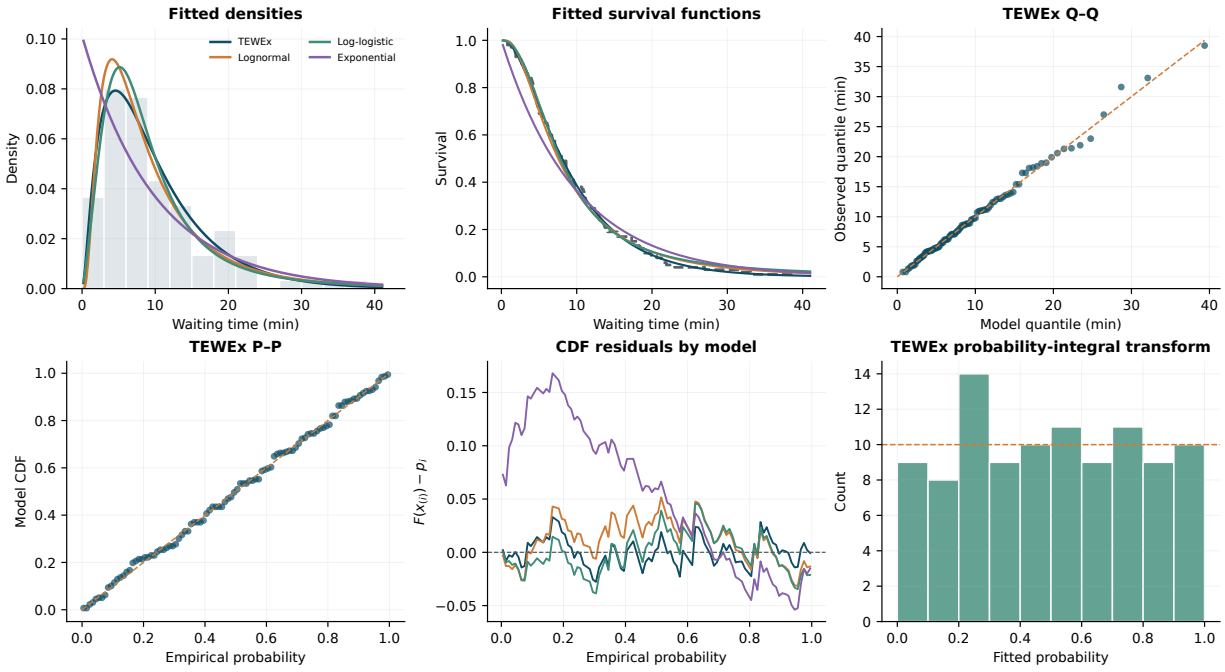


Figure 9. Fitted model diagnostics for data.

Figure 10 displays conditional likelihood slices, obtained by varying one parameter while holding the other three at the fitted values. These are not nuisance-parameter-optimized profile likelihoods and should not be used as confidence limits. The vertical axis shows the conditional log likelihood relative to its maximum on the plotted range, so the peak is upward in every panel. Figure 11 shows the corresponding pairwise conditional contours and highlights parameter dependence.

The complete-sample TEWEx posterior uses the real-data priors in (39), which differ from the fixed Log-MAP prior in the simulation section. Two independently initialized HMC chains, each with 1,200 warm-up and 2,200 retained draws, provide the posterior summaries in Table 13. The credible ranges summarize posterior uncertainty under the stated real-data prior and are interpreted alongside the chain diagnostics.

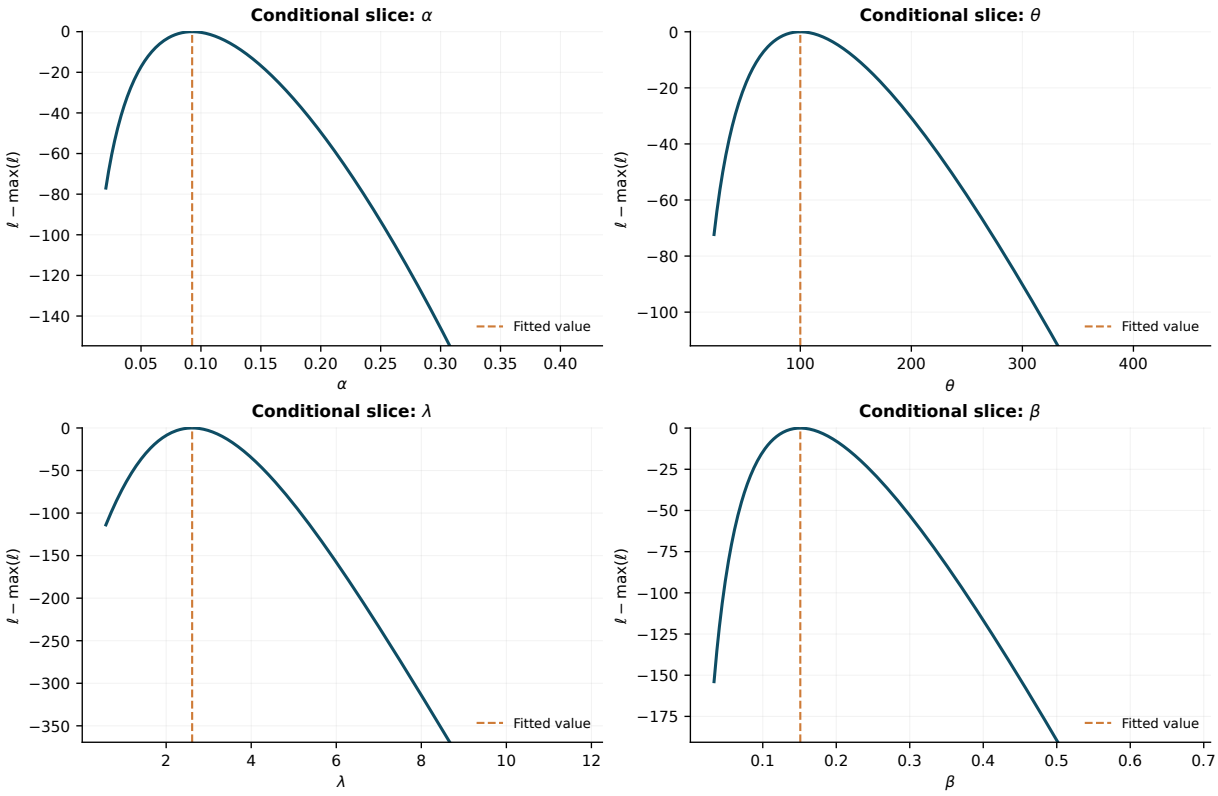


Figure 10. Conditional TEWEx log-likelihood slices.

Table 13. Data posterior summaries.

Parameter	Posterior mean	2.5%	97.5%	$\widehat{R}$	ESS
α	2.485	0.219	10.176	1.000	4400
θ	2.664	0.192	12.056	1.000	4400
λ	0.723	0.041	2.890	1.000	855
β	0.145	0.095	0.187	1.000	4400

Figure 12 displays the two-chain parameter traces; Figure 13 illustrates the skewed posterior marginals of the shape parameters relative to the more concentrated baseline-rate posterior; and Figure 14 presents the corresponding lag-dependent sampling correlations.

Let $n = 100$ denote the original lifetime data sample size. The four specified configurations $\{(r, T) = (70, 8), (90, 8), (70, 15), (90, 15)\}$ are re-evaluated by the actual rule $C = \min\{T, X_{(r)}\}$. In particular, $(70, 8)$ and $(90, 8)$ terminate at the same time before either failure threshold is reached; they must have the same observed sample, likelihood, and estimates. Their realized observation patterns are summarized in Table 14. The hybrid

Table 14. Observed hybrid-censoring patterns for data.

r	T	C	Observed failures d	Stopping event
70	8	8.00	50	Time
90	8	8.00	50	Time
70	15	11.50	70	Failure
90	15	15.00	81	Time

experiment therefore changes the amount of information available for inference; its results must be computed from d observed failure times and $n - d$ survivors at C through (40). In particular, the complete-sample HMC figures above are *not* presented as hybrid-censored posterior figures. The distinction keeps the likelihood, observation scheme, and posterior diagnostics aligned.

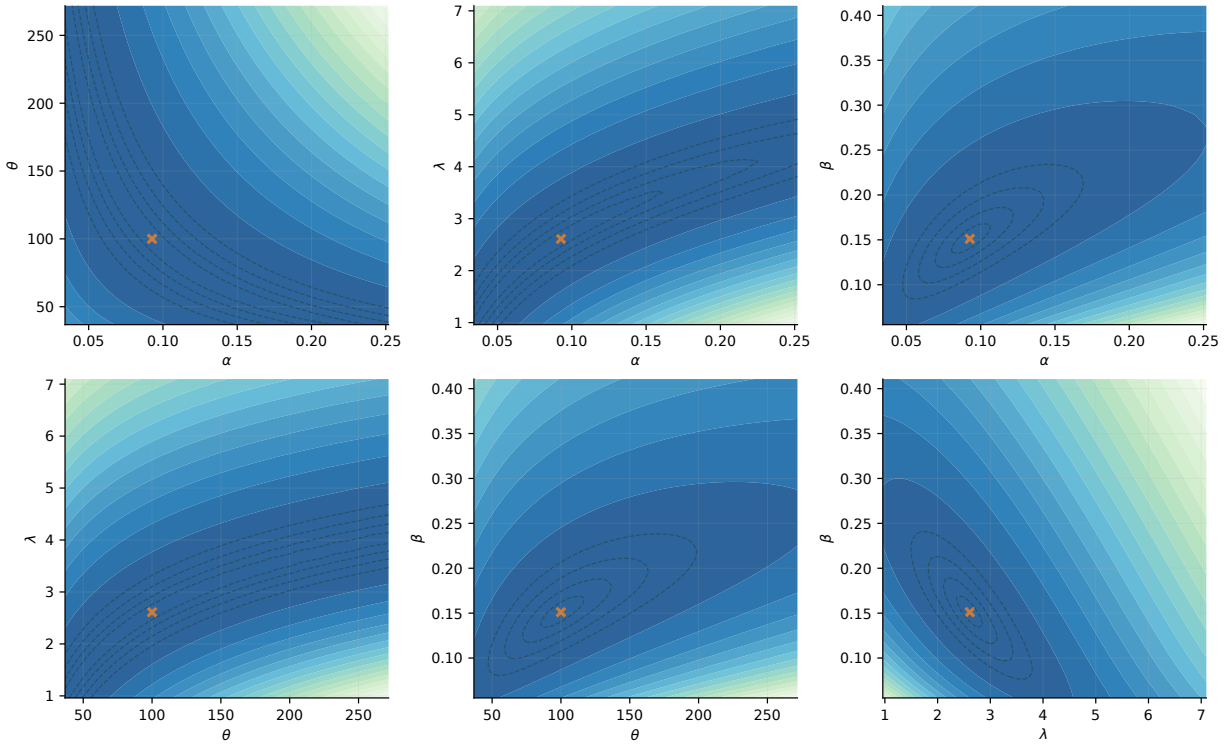


Figure 11. Conditional log-likelihood contours for TEWEx.

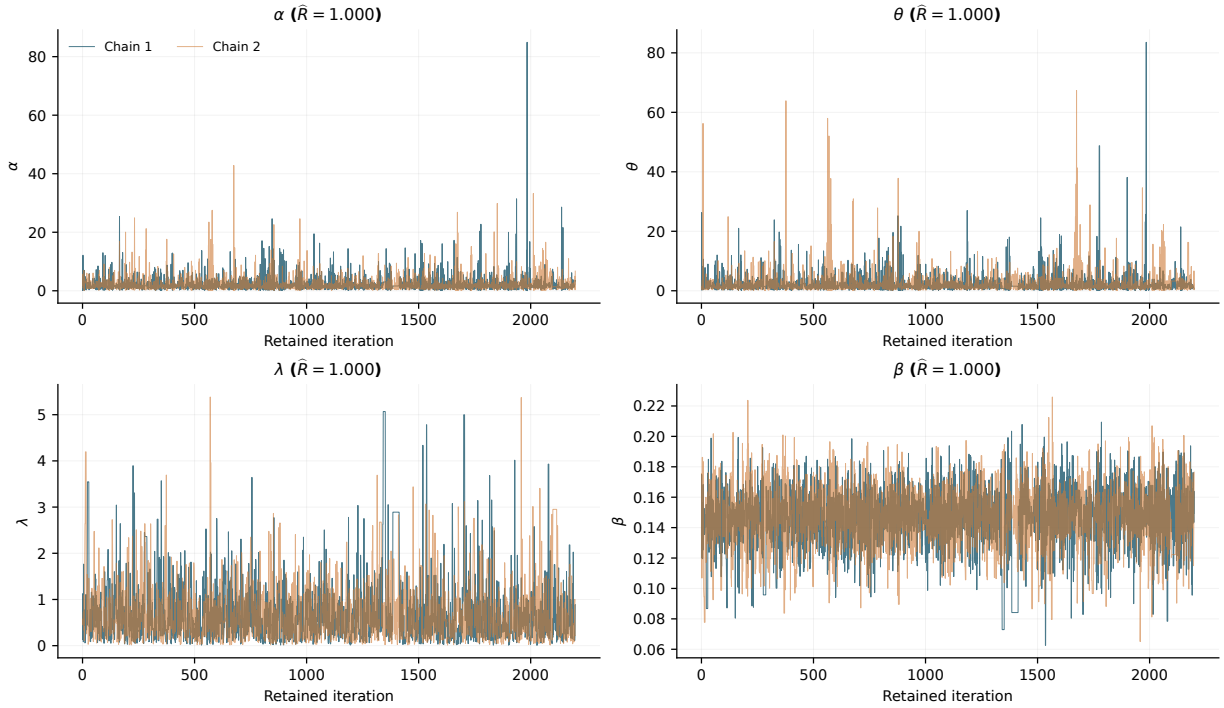


Figure 12. HMC traces for the data TEWEx parameters.

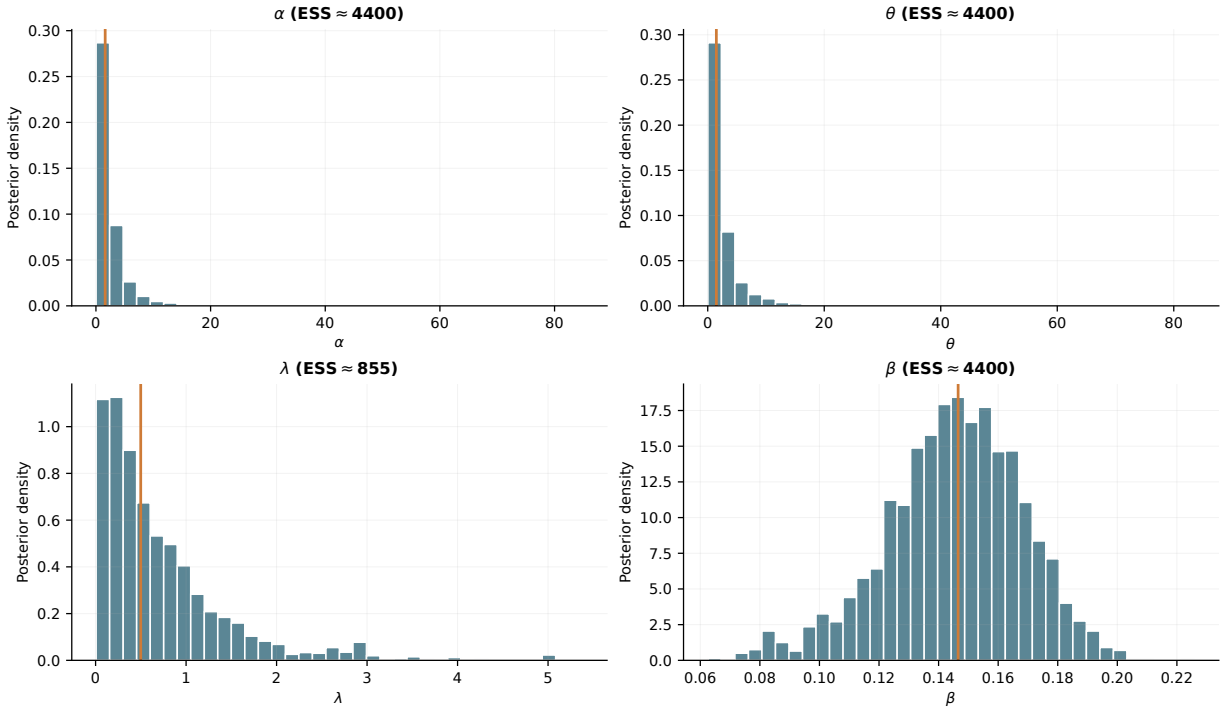


Figure 13. Posterior densities for the data TEWEx parameters.

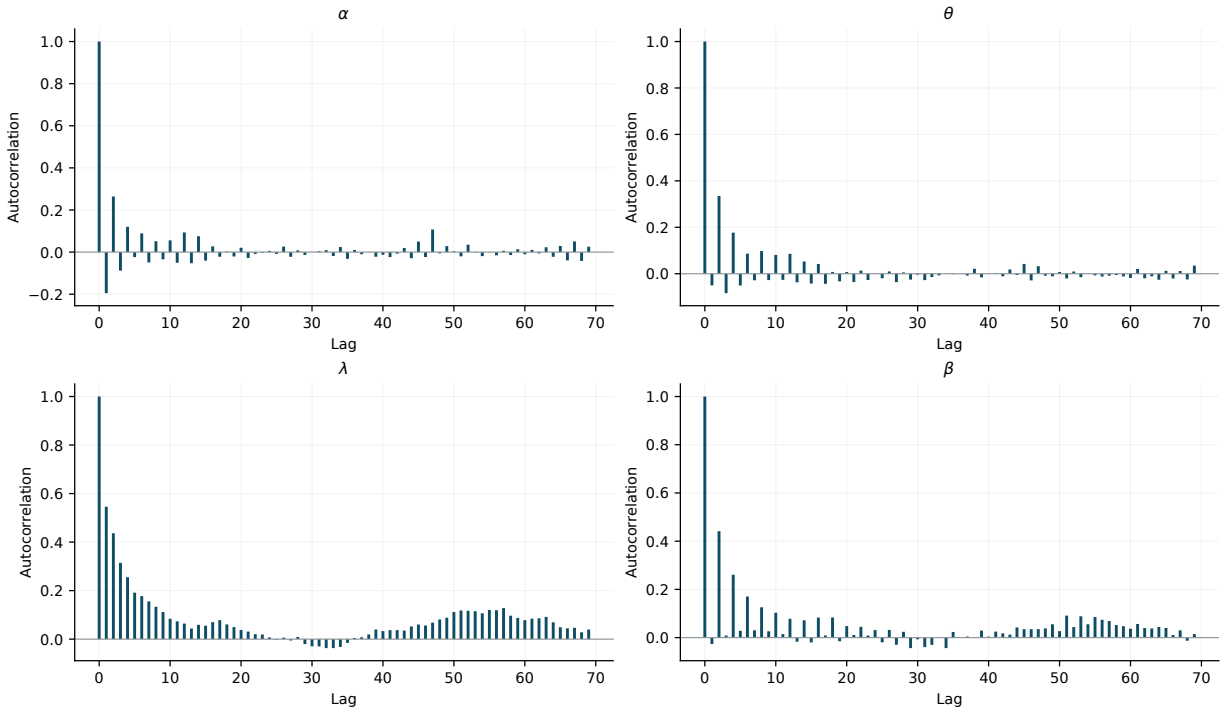


Figure 14. HMC autocorrelation for the data parameters.

7. Conclusion and Roadmap

This paper introduced the truncated exponentiated Weibull-G (TEW-G) family and developed its density, hrf, moments, reliability measures, entropy functionals, and selected characterizations. The exponential, Rayleigh and Lindley baselines illustrated the construction. The family produces monotone and non-monotone hazard shapes, including increasing, decreasing, bathtub, unimodal, J-shaped and inverse-J-shaped, and it accommodates symmetric and asymmetric densities with different levels of kurtosis. The Monte Carlo study used $48{,}000$ datasets across four parameter configurations, four sample sizes, three observation regimes (complete data and two Type-I hybrid-censoring levels) and $1{,}000$ replications per cell. It shows that this flexibility carries a finite-sample cost. The fitted cdf is recovered reasonably well in several regimes even when individual shape parameters are poorly separated. MLE boundary solutions average 37.7%, falling from 57.1% at $n = 50$ to 20.2% at $n = 400$. Numerically admissible observed-information log-Wald intervals exist in only 61.3% of replications on average, rising from 42.3% to 77.9% over the same range of n. Coverage conditional on availability therefore cannot be read as evidence of reliable frequentist inference. The regularised posterior mode in log-parameter coordinates (Log-MAP) gave a smaller cdf-grid RMSE than the MLE in all 48 of 48 cells (mean 0.0374 against 0.0396). This is a result specific to this experiment and prior, not a general claim about Bayesian estimators, and parameter-level identifiability under censoring remained difficult. The lifetime application with the exponential-baseline model, compared with three reference distributions through information criteria and refitted parametric-bootstrap Kolmogorov–Smirnov p-values, illustrates flexible fitting. A good fit should not be read as precise identification of every parameter, so we recommend reporting fitted-distribution quantities together with boundary incidence, censoring fractions and interval availability. These conclusions are conditional on the configurations, baseline, censoring levels and single fixed prior studied, and on one dataset. Future work should therefore start with the analytical Fisher information, to establish identifiability conditions and find reparameterisations that reduce boundary solutions. It should then evaluate profile-likelihood, bootstrap and calibrated credible intervals, together with prior sensitivity and objective priors. Further directions are Type-II, progressive, interval and competing-risks censoring, including a spacing-based criterion under censoring, and regression and frailty extensions on the truncated support. They also include other baselines with model-selection and goodness-of-fit performance, robust and better-initialised computation, and bivariate, copula-based and discrete versions of the family.

Acknowledgments

The authors extend their appreciation to Prince Sattam bin Abdulaziz University for funding this research work through the project number (PSAU/2025/01/35309).

Data Availability

The dataset is included within the paper.

Conflict of Interest

The authors have disclosed no conflicts of interest.

REFERENCES

1. Aban, I. B., Meerschaert, M. M. and Panorska, A. K. (2006). Parameter estimation for the truncated Pareto distribution. *Journal of the American Statistical Association*, **101**, 270–277.
2. Abdelall, Y. Y., Hassan, A. S. and Almetwally, E. M. (2024). A new extension of the odd inverse Weibull-G family of distributions: Bayesian and non-Bayesian estimation with engineering applications. *Computational Journal of Mathematical and Statistical Sciences*, **3**(2), 359–388.

3. Ahmed, S. E., Castro-Kuriss, C., Flores, E., Leiva, V. and Sanhueza, A. (2010). A truncated version of the Birnbaum–Saunders distribution with an application in financial risk. *Pakistan Journal of Statistics*, **26**(1), 293–311.
4. Almetwally, E. M., Metwally, D. S. and Elbatal, I. (2025). A new statistical model for inflation risk evaluation using actuarial techniques. *Annals of Data Science*, 1–33. https://doi.org/10.1007/s40745-025-00644-6
5. Atchadé, M. N., Agbahide, A. A., Otodji, T., Bogninou, M. J. and Moussa Djibril, A. (2025). A new shifted Lomax-X family of distributions: properties and applications to actuarial and financial data. *Computational Journal of Mathematical and Statistical Sciences*, **4**(1), 41–71.
6. Bashir, S., Masood, B., Al-Essa, L. A., Sanaullah, A. and Saleem, I. (2024). Properties, quantile regression, and application of bounded exponentiated Weibull distribution to COVID-19 data of mortality and survival rates. *Scientific Reports*, **14**, art. 14353.
7. Burroughs, S. M. and Tebbens, S. F. (2002). The upper-truncated power law applied to earthquake cumulative frequency-magnitude distributions. *Bulletin of the Seismological Society of America*, **92**, 2983–2993.
8. Cheng, R. C. H. and Amin, N. A. K. (1983). Estimating parameters in continuous univariate distributions with a shifted origin. *Journal of the Royal Statistical Society, Series B (Methodological)*, **45**(3), 394–403.
9. Elghaly, H. E., Abd Elgawad, M. A. and Tian, B. (2025). A novel extension to the unit Weibull distribution: properties and inference with applications to medicine, engineering, and radiation. *AIMS Mathematics*, **10**(8), 18731–18769.
10. Eliwa, M. S., & El-Morshedy, M. (2020). Bivariate odd Weibull-G family of distributions: Properties, Bayesian and non-Bayesian estimation with bootstrap confidence intervals and application. *Journal of Taibah University for Science*, *14*(1), 331–345.
11. El-Morshedy, M., Eliwa, M. S., & Tyagi, A. (2022). A discrete analogue of odd Weibull-G family of distributions: Properties, classical and Bayesian estimation with applications to count data. *Journal of Applied Statistics*, *49*(11), 2928–2952.
12. El-Morshedy, M., Alshammari, F. S., Tyagi, A., Elbatal, I., Hamed, Y. S., & Eliwa, M. S. (2021). Bayesian and frequentist inferences on a type I half-logistic odd Weibull generator with applications in engineering. *Entropy*, *23*(4), Article 446.
13. El-Morshedy, M., & Eliwa, M. S. (2025). Discrete double factors of a family of odd Weibull-G distributions: Features and modeling. *International Journal of Data Science and Analytics*, *20*, 1–24.
14. Shahen, H., El-Morshedy, M., & Eliwa, M. S. (2026). Discrete odd Weibull-Lindley distribution featuring adaptable hazard rate and dispersion index: Theoretical framework and applications to SDG-aligned count data. *Statistics, Optimization & Information Computing*. https://doi.org/10.19139/soic-2310-5070-4736
15. El-Morshedy, M., Elbatal, I., Harpy, M. H., & Eliwa, M. S. (2026). Theory-Driven Inference and Data Modeling for the Odd Weibull-G Negative Binomial Class. *Statistics, Optimization & Information Computing*. Advance online publication. https://doi.org/10.19139/soic-2310-5070-4736
16. El-Morshedy, M., & Eliwa, M. S. (2023). A bivariate extension to exponentiated inverse flexible Weibull distribution: Shock model, features, and inference to model asymmetric data. *Symmetry*, *15*, Article 411.
17. Eugene, N., Lee, C. and Famoye, F. (2002). Beta-normal distribution and its applications. *Communications in Statistics—Theory and Methods*, **31**, 497–512.
18. Glänzel, W. (1987). A characterization theorem based on truncated moments and its application to some distribution families. In *Mathematical Statistics and Probability Theory* (Bad Tatzmannsdorf, 1986), Vol. B, Reidel, Dordrecht, 75–84.
19. Glänzel, W. (1990). Some consequences of a characterization theorem based on truncated moments. *Statistics: A Journal of Theoretical and Applied Statistics*, **21**(4), 613–618.
20. Gupta, P. L. and Gupta, R. C. (1983). On the moments of residual life in reliability and some characterization results. *Communications in Statistics—Theory and Methods*, **12**(4), 449–461.
21. Hamedani, G. G. (2013). Characterizations of exponentiated distributions. *Pakistan Journal of Statistics and Operation Research*, **9**(1), 17–24.
22. Hassan, A. S., Abdalla, G. S. S., Elgarhy, M., Mendy, J. T. and Almetwally, E. M. (2025). Efficient inference of $P(W < Z)$ using ranked set sampling: the inverse power half-logistic model. *Journal of Statistics Applications & Probability*, **14**(5), 761–785.
23. Jamal, F., Bakouch, H. and Nasir, M. A. (2021). A truncated general-G class of distributions with application to truncated Burr-G family. *REVSTAT—Statistical Journal*, **19**(4), 513–530.
24. KrishnaKumari, K. and George, D. (2025). A new left truncated distribution for modeling failure time data: estimation, robustness study and application. *Statistics, Optimization & Information Computing*, **13**(6), 2264–2277.
25. Mudholkar, G. S. and Srivastava, D. K. (1993). Exponentiated Weibull family for analyzing bathtub failure rate data. *IEEE Transactions on Reliability*, **42**, 299–302.
26. Najarzadegan, H., Alamatsaz, M. H. and Hayati, S. (2017). Truncated Weibull-G more flexible and more reliable than beta-G distribution. *International Journal of Statistics and Probability*, **6**(5), 1–17.
27. Navarro, J., Franco, M. and Ruiz, J. M. (1998). Characterization through moments of the residual life and conditional spacings. *Sankhyā: The Indian Journal of Statistics, Series A*, **60**(1), 36–48.
28. Obakeng-Maphane, T., Oluyede, B., Chipepa, F. and Tlhaloganyang, B. (2026). A new flexible Marshall–Olkin extended odd Weibull-G family of distributions: theory, properties and applications. *Statistics, Optimization & Information Computing*, **15**(6), 4635–4681.
29. Pal, M., Ali, M. M. and Woo, J. (2006). Exponentiated Weibull distribution. *Statistica*, **66**(2), 139–147. https://doi.org/10.6092/issn.1973-2201/493.
30. Shanker, R., Hagos, F. and Sujatha, S. (2016). On modeling of lifetime data using one parameter Akash, Lindley and exponential distributions. *Biometrics & Biostatistics International Journal*, **3**(2), 56–62.
31. Singh, S. K., Singh, U. and Sharma, V. K. (2014). The truncated Lindley distribution: inference and application. *Journal of Statistics Applications & Probability*, **3**(2), 219–228.
32. Zaninetti, L. and Ferraro, M. (2008). On the truncated Pareto distribution with applications. *Central European Journal of Physics*, **6**(1), 1–6.
33. Zhang, T. and Xie, M. (2011). On the upper truncated Weibull distribution and its reliability implications. *Reliability Engineering and System Safety*, **96**, 194–200.